THESIS

METHODS FOR PARTICULATE MATTER EMISSIONS REDUCTION IN WOOD BURNING COOKSTOVES

Submitted by

Kevin Dischino

Department of Mechanical Engineering

In partial fulfillment of the requirements

For the Degree of Master of Science

Colorado State University

Fort Collins, Colorado

Spring 2015

Master's Committee:

Advisor: Anthony Marchese

Jeffrey Pierce
John Volckens

ABSTRACT

METHODS FOR PARTICULATE MATTER EMISSIONS REDUCTION IN WOOD BURNING COOKSTOVES

About 3 billion people cook by burning biomass. Most use inefficient cooking technologies that lead to high levels of domestic air pollution. This results in tremendous damages to human and environmental health. For example, in 2012 the World Health Organization estimated that 4.3 million people died prematurely from illnesses attributable to inefficient household use of biomass fuels.

Colorado State University's cookstove laboratory has challenged this global problem by developing technology that reduces Particulate Matter (PM) emissions by over 80% from wood burning rocket elbow cookstoves, and by over 90% from traditional cookstoves.

To achieve this reduction, the effects of exhaust gas recirculation and ambient air injection on PM emissions were evaluated experimentally. Exhaust gas recirculation significant decreases in PM emissions through the mechanisms of oxygen and particle recirculation, and enhanced mixing. However, for the case of the approximately 3kW rocket elbow cookstoves, ambient air injection was found to outperform exhaust gas recirculation.

In order to design air injection technology that effectively reduced emissions, significant effort was put towards optimization of the injection location, injection angle, nozzle geometry and flow rates. Ultimately, a robust and effective air injection design that approaches IWA Tier 4 PM pollution standards is recommended for use in a commercial product

TABLE OF CONTENTS

LIST OF TABLES

LIST OF FIGURES

1 Introduction

1.1 Traditional to Improved Cookstoves: Brief Overview

Evidence of the first controlled use of fire dates back 500,00 years, with some evidence generating claims that humans controlled fire up to 1.7 million years ago [1]. Harnessing this technology opened the doors to societal growth years ago and continues to sustain much of our society today. From transportation, to cooking, heating, manufacturing, and much more, we rely on combustion. Despite our reliance on combustion, some of its applications have yet to be optimized for reduction of human and environmental health impacts. One of these particular applications is the combustion of biomass for cooking.

Currently, around 3 billion people cook by burning biomass and coal [2]. Moreover, for the past 12,000 years, the main method of cooking was with the inefficient three-stone fire, also known as the traditional stove, seen below.

Figure 1. Traditional Cookstove

Advancements in cooking technology have only recently been realized. In the 1950's Gandhian organizations in India initiated cookstove technology development. By the late

1970’s and early 1980’s, significant scientific research and development in the field of Improved Cookstoves (ICS) was underway [1]

An improved cookstove differs from a traditional cookstove via two main facets. First, an improved cookstove delivers heat to the food more efficiently than a three stone fire. Second, an improved cookstove will have lower emissions per unit of energy delivered to the food than a three stone fire. An example of an improved cookstove is the wood-burning rocket-elbow stove. The geometry of a rocket elbow stove induces a natural draft that promotes clean combustion and higher thermal efficiency. The Envirofit M5000 is a current example of a rocket elbow stove that is used around the world.

Figure 2. Improved Cookstove

The emissions that are released from biomass cookstoves include carbon monoxide and particulate matter. Particulate matter emissions are of great concern, as they can have a significant detrimental effect on atmospheric visibility, global climate, and long term human health [3]. Although improved cookstove designs can lead to significant reductions in emissions when compared to traditional cookstoves, most improved cookstoves still do not emit at levels that are deemed acceptable by WHO indoor air pollution standards. Subsequently, the World Health Organization states that in 2012, over 4 million people died prematurely from illnesses attributable to household air pollution caused by inefficient use of solid biomass fuels.

Particulate Matter (PM) alone can be blamed for more than 50% of premature deaths among children under 5 years old[2].

In an effort to reduce the global problem of inefficient and dirty combustion of biomass, CSU's cookstove laboratory has developed an emissions reducing technology that is applicable to a commonly used wood-burning rocket elbow cookstove.

1.2 Project Background

In 2013, Research Triangle Institute was awarded a research grant through the Department of Energy with the abridged goals of developing an affordable add-on device to enhance rocket elbow cookstove performance to approach IWA Tier 4 levels and then to bring this technology to market in a safe, reliable, and effective manner. Research Triangle Institute partnered with Colorado State University (CSU) and Envirofit for this project. Colorado State University's primary role was the exploration, optimization and understanding of various means of reducing emissions from the Envirofit M-5000 rocket elbow. Additionally, collaboration between Envirofit and Colorado State University under a Small Business Innovation and Research grant allowed for further exploration of the emissions reducing methods for the Envirofit G3300 rocket elbow stove.

Two main emissions reducing methods were explored through approximately 500 hours of experimental work. The first method utilized exhaust gas recirculation, a novel technique for biomass cookstoves. The second method utilized ambient air injection. In Figure 3 the general principles of these two emissions reducing techniques are seen.

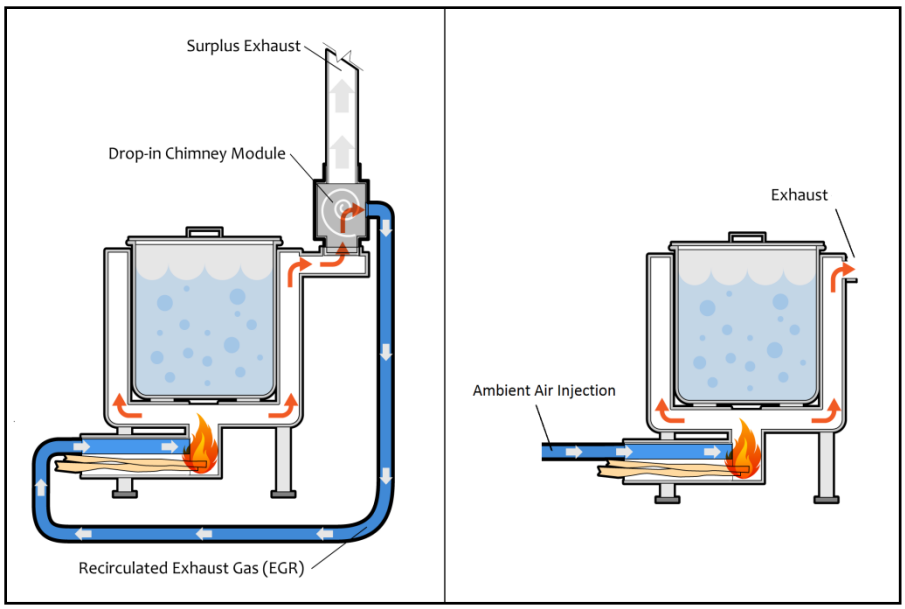

Figure 3. Emissions Reduction Approaches

2 Cookstoves Emissions Technical Discussion

A general background of biomass cookstove emissions and emissions measurement is provided, with added focus on the wood-burning rocket elbow cookstove.

2.1 Cookstove Emissions Characterization

In 2012 an International Workshop Agreement (IWA) was affirmed by the global cookstoves community that provided guidance for ranking cook stove performance in the categories of fuel use/efficiency, total emissions, indoor emissions, and safety. "Tiers of Performance" ranging from Tier 0 to Tier 4 provide the basis for ranking and comparison of stoves. Tier 0 is defined by poorly performing traditional open fire stoves, whereas Tier 4 is defined by ambitious health and or environmental-related targets. Typically, liquid and gas fuel stoves (e.g. ethanol and LPG) are the only stoves that consistently meet Tier 4 standards. The results of a stove performance inventory report completed by the Berkley Air Monitoring Group in 2012 help to illuminate general performance of various cookstoves with respect to the IWA Tiers for emissions [4].

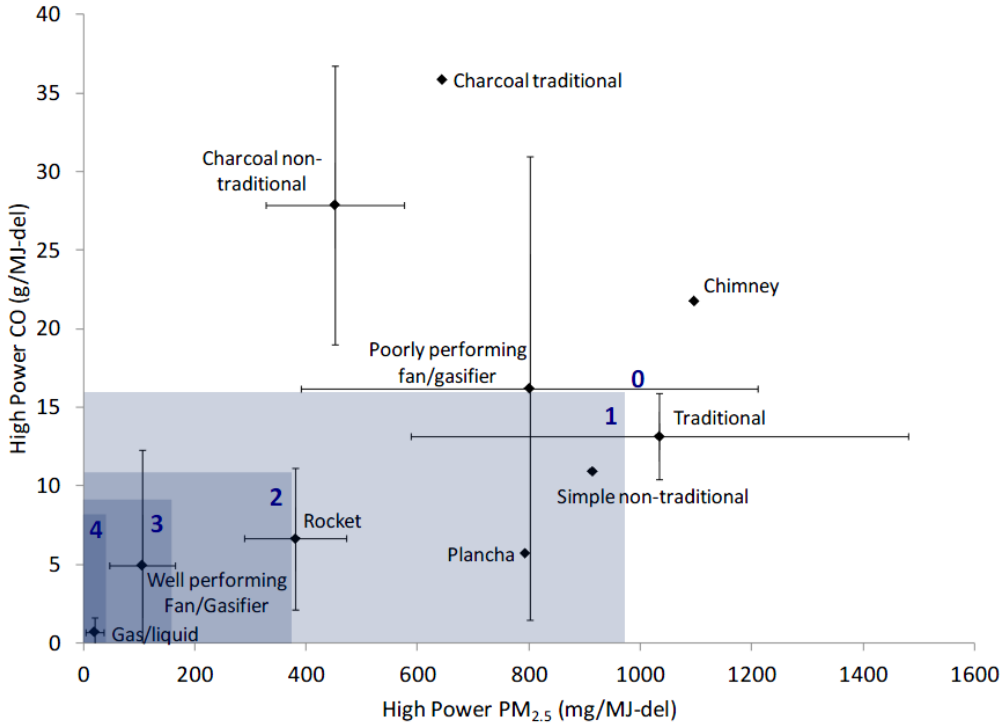

Figure 4. Berkley Air Monitoring Group Stove Performance Report

The IWA Tiers for carbon monoxide and particulate matter emissions are outlined in Figure 4. Typical rocket elbow stove is reported to have Tier 1 performance in the PM emissions category, and Tier 4 performance in the carbon monoxide emissions. Consequently, this study focuses primarily on the reduction of PM emissions from a rocket elbow cookstove.

2.2 PM Formation, Growth, and Oxidation in Biomass Combustion

In order to measure PM emissions and to develop PM emissions reducing cookstove technology, it is critical to first acquire an understanding of the current scientific knowledge of PM formation, growth and oxidation in biomass combustion. There are four main classes of particles that are emitted during biomass combustion. These include soot and inorganic particles that are produced at high temperatures, and H_2SO_4 and condensable organics particles that are produced at exhaust temperatures [5].

The inorganic elements typically found in biomass fuels, such as calcium, potassium and other minerals, are unlikely to oxidize to gas phase compounds during wood combustion. Therefore the majority of these inorganic compounds will remain as PM emissions [6]. Even if these inorganic elements do oxidize, many of the resulting inorganic vapors (e.g., metal oxides) have an exceedingly small vapor pressure even at high temperatures. Thus, they would nucleate out of the gas quickly in a sooting flame [3]. The nucleation of inorganic particles can contribute to condensation sites for soot particles.

The formation and oxidation of soot can be characterized by three main regions: 1) Particle inception region, 2) Surface growth region, 3) Oxidation region. In the particle inception region, particle number density increases and soot volume fraction increaseS while primary size is kept small. In the surface growth region particle number density is relatively constant while primary particle size and soot volume fraction increase primarily due to condensation of growth species, C_2H_2 (acetylene), and/or PAH (Polycyclic Aromatic Hydrocarbon) on the soot particle surface. In the oxidation region soot volume fraction and soot particle size decrease due to the attack of soot particles by OH an O radicals [7].

Boundaries between these three regions are not distinct and overlap can exist depending on local conditions. However, their general location can be described. The particle inception and surface growth regions exist in fuel rich zones, because hydrocarbon fragments have a greater chance of colliding with other hydrocarbon fragments and growing, rather than being oxidized. The soot volume fraction within these fuel rich zones is initially high, but much of the soot is subsequently destroyed in the flame by oxidation, and soot emissions are much lower than the initial soot volume fraction that occurs in fuel-rich zones [5]. It is likely that the bulk of the particle inception region exists very close to the solid fuel within the pyrolysis products and prior to significant exposure to oxidizers and combustion.

The soot oxidation region generally exists in high temperature regions of the flame. More specifically, in flame temperatures over 800^{o}C, formation of soot competes with oxidation of soot [8, 15]. The oxidation region is clearly visualized in a flame as the incandescent regions that form as carbonaceous particles are oxidized.

2.3 General Testing Methodology

Overviews of emissions measurement techniques, equipment and emissions related testing protocols are provided below.

2.3.1 Emissions Measurement Equipment

The emissions sampling systems at the Advanced Cookstoves Laboratory are the result of collaborations between various experts in the fields of aerosol and emissions sampling. $PM_{2.5}$ emissions were measured using a gravimetric sampling system. The gravimetric system utilized a URG Corporation cyclone with a 2.5 micron cutpoint. Volumetric flow rate through the cyclone was controlled with an Alicat Flow Controller. Compensation for changes in the flue gas density (due to increasing pressure drop across the filter and changes in flue gas temperature) was performed at 1 second intervals, allowing for active volumetric control of the flow through the cyclone. $PM_{2.5}$ mass emissions are collected on Pallflex filters and weighted using a scale with 1 microgram of precision. Electrical resistance heater tape and a temperature controller were used to ensure that that sampling of PM in the cyclone was completed isothermally, at a temperature of 115^{o} Fahrenheit. Gaseous emissions, including carbon monoxide and carbon dioxide, were measured with a Siemens Ultramat 6 gas analyzer and a Testo 350 gas analyzer.

2.3.2 Repeatability Protocols for $PM_{2.5}$ Emissions

Despite accurate and reliable PM measurement equipment, significant variation in PM is often observed. Thus, $PM_{2.5}$ source emissions from biomass combustion are variable and difficult to control. In order achieve greater confidence in data, variables that have an influence on the produced emissions were held constant throughout the study. These variables are as follows:

- Stove condition
- Fuel characteristics
- Firepower

Stove Condition: The Global Alliance for Clean Cookstoves calls for the "seasoning" of stoves before measurement, because a new stove may perform differently than a used stove [9]. For example, a new stove may have oils leftover on its surfaces from manufacturing processes, potentially changing $PM_{2.5}$ emissions. However, the stove condition should also be maintained at a constant after it has been seasoned. This necessitated a pre-test protocol which involved vacuuming loose char and dust from the stove chamber, outer body, and outside of the pot.

Fuel: Fuel composition, surface area, and spacing are critical variables that affect $PM_{2.5}$ emissions, and must be maintained constant. The fuel composition and geometry utilized throughout the study was pine shims for the "start-up" phase and acacia ½"x ½" x 12" trim board for the "steady-state" phase. Quality control for the shims was ensured by cutting them in house from 2"x12" pine boards. Fuel spacing was kept constant at ½" using a frame attached to the fuel grate of the cookstove. The effect of fuel spacing is discussed further in section 3.2.2.

Firepower: Firepower was maintained constant by keeping the end of the sticks at approximately ½" from the back of the combustion chamber. However, firepower is difficult to

maintain at a constant rate. The effect of firepower on $PM_{2.5}$ emissions is discussed further in Section 3.2.3 and a correction for firepower variations is proposed in Section 3.4.

Additionally, there are variables that are intrinsic to $PM_{2.5}$ measurement, such as fluctuations in background $PM_{2.5}$ concentration, process error associated with handling of filters and collection of moisture on filters. In order to reduce error associated with these variables the following steps were taken:

- Daily background $PM_{2.5}$ concentration measurements
- Conditioning of filters before/after each test in a constant humidity/temperature environment
- Quantification of mass deposition on filter associated with handling the filter (process error)
- Quantification of Limit of Detection and Limit of Quantification

2.3.3 Limit of Detection/Limit of Quantification

In order to better understand the limitations associated with the weighing of the $PM_{2.5}$ mass deposited on the filters from gravimetric system, tests were completed to determine the Limit of Detection (LOD) and Limit of Quantification (LOQ). The LOD is defined as the lowest value that a process can reliably detect. The definition of the term "reliable" is somewhat loose, but it is generally recommended that the LOD is located at three standard deviations above the blank signal, as seen in Equation 1.

$$\boldsymbol{LOD = 3\sigma + Blank\ Signal} \qquad \text{Equation 1}$$

The LOQ is defined as a region significantly above the LOD, where quantification of the measured value is possible. It is recommended that the LOQ be located 10 standard deviations above the blank signal, as seen in Equation 2 [10].

$$LOQ = 10\sigma + Blank\ Signal$$ Equation 2

In order to measure the LOD and LOQ, a blank filter was weighed before and after any handling that occurs when collecting a PM measurement with the gravimetric sampling system, for 7 trials. This data is pictured below in Table 1.

Table 1. LOD and LOQ data

Trial #	Blank Filter Weight Difference (µg)
1	12.7
2	18.0
3	13.3
4	4.0
5	10.0
6	5.3
7	4.3

The results of the LOD and LOQ calculation can be seen below in Table 2.

Table 2. LOD and LOQ results

Average Blank Signal (µg)	9.7
Standard Deviation (µg)	5.3
LOD (µg)	26
LOQ (µg)	63

2.3.4 Statistical Methods

Various statistical analyses were used to analyze emissions data collected in this study. A brief overview of the statistical methods used in this study is provided below.

Confidence Interval: A confidence interval displays range in which a population mean likely exists, to some degree of confidence. In the calculation of confidence intervals throughout this document, a t-distribution is used, a more appropriate distribution for small sample sizes, along

with a confidence level of 80%. Error bars found throughout this document indicate an 80% confidence interval calculated using a t-distribution, a more appropriate distribution for small sample sizes.

Two-Sample t-test: A two sample t test is a hypothesis test for difference between two sample means. It assumes that the population for each sample is normally distributed and that the samples are independent [11]. Two sample, two tailed t-tests assuming unequal variances between the samples are used throughout this document to prove statistically significant difference between sample means. A significance level of 5% is used as the threshold to judge the validity of the hypothesis for all t-tests in this study. T-tests are qualitative indicators of a statistically significance difference between samples, but not of the magnitude of difference. Therefore if a t-test indicates a statistically significant difference between sample means, then a percent reduction from baseline is also reported to quantify the magnitude of difference.

Coefficient of Variation: This is a dimensionless metric, ranging from 0 to 1, that is used to gauge the extent of variability of a sample relative to its mean. The coefficient of variation is useful for the comparison of dispersion of independent sample sets [11].

3 Baseline Cookstove Testing

Two different cookstoves were used as the platform for experimentation throughout the study, including the Envirofit M5000 and the Envirofit G3300 stoves. The M5000 is pictured in Figure 5 and the G3300 is pictured in Figure 6.

Figure 5. Envirofit M5000 Wood-Burning Rocket Elbow Cookstove

Figure 6. Envirofit G3000 Wood-Burning Rocket Elbow Cookstove

Both of these stoves are side-feed natural draft rocket elbow cookstoves. The M5000, used in sections 3 through 7 of this study, has a metallic chamber, a ceramic base that occupies the entire bottom area of the stove, and an aluminum foil heat shield around the combustion chamber. The G3300, used in sections 8 through 11 of this study, has a metallic combustion

chamber with a slightly larger mouth, a ceramic base that occupies only the bottom area of the combustion chamber, and fiberglass insulation. In Section 3, the baseline performance metrics for both stoves are quantified. Additionally, given the inherently variable nature of $PM_{2.5}$ emissions from biomass combustion, a significant effort was made towards identifying parameters that may significantly influence these baseline $PM_{2.5}$ emissions.

3.1 Testing Methodology

Described in this section are the methodologies used to determine the baseline stoves' performance metrics, and the effects of pot skirt, stick spacing and firepower on $PM_{2.5}$ emissions and thermal efficiency.

3.1.1 GACC Protocols

All tests specified as "cold start water boil tests" throughout this document were completed in accordance with the Global Alliance for Clean Cookstoves WBT Phase 1 protocol [11]. Additionally, all calculations of stove performance metrics were completed in accordance with GACC protocols. If not specified as a "cold start water boil test", other testing procedures were used and will be outlined accordingly.

3.1.2 Pot Skirt

A pot skirt was utilized throughout all tests included in this study. The potskirt was constructed from thin stainless steel, and was sized such that the area of the gap around the pot matched the area of the chimney portion of the rocket elbow stoves. The effect of the pot skirt was measured by comparing the baseline data from this study with stove certification test data previously compiled at the CSU Cookstoves Laboratory that did not use a pot skirt.

3.1.3 Stick Spacing

Testing of the effect of fuel stick spacing was accomplished by use of a frame incorporated into the fuel grate of the M5000, pictured below in Figure 7.

Figure 7. Stick Spacing Frame

The M5000 fuel grate is curved, causing sticks to tend to slide together, decreasing the spacing and increasing variability in the testing procedure. The stick spacing frame, helped to mitigate this issue by supporting three sticks in a parallel formation at ½ inch spacing. In order to test the effect of ½ inch stick spacing, two sets of three replicate cold start tests were performed. In the first set, stick spacing was not controlled, and in the second set stick spacing was controlled.

3.1.4 Firepower

The effect of firepower on cold start $PM_{2.5}$ emissions was tested by running 9 cold start tests on the M5000, using 3 different fuel feeding approaches with 3 replicates each. Specifically, in the steady state-phase of the test, upon completion of burning of the shims, either 2, 3, or 4 sticks were fed simultaneously.

Additionally, testing was completed to better understand the relationship between $PM_{2.5}$ emissions and firepower within the duration of a cold start. To accomplish this, pseudo real-time $PM_{2.5}$ mass flow data was collected for three cold start tests using a 3 stick feed rate on the M5000.

3.1.5 Correlation for Particulate Mass Loading on Filter

In order to measure the pseudo real-time mass loading of $PM_{2.5}$ on the filter in the gravimetric sampling system, a correlation was developed between mass load and pressure drop across the filter. The derivation of this correlation is described below.

During a simmer test, all variables that influence PM mass flow rate are held relatively constant. Therefore the mass flow rate of PM during a simmer test is constant. A linear relationship between mass loading of PM on the filter and pressure drop across the filter was observed during 45 minute simmer tests of a natural draft rocket elbow cookstove, indicating that the pressure drop across the filter is a linear function of mass loading for this particular scenario. The results of these simmer tests can be seen below in Figure 8.

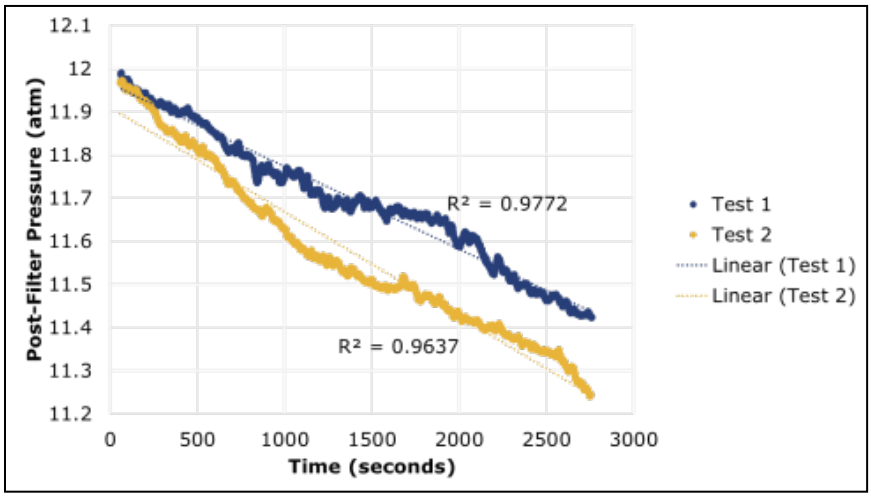

Figure 8. Simmer Test Pressure Drop Across Filter

The observed linear increase in pressure drop as a function of time led to the development of Equation 3, used to determine cumulative mass on the filter from the pressure drop data.

$$\boldsymbol{Filter\ Mass\ Loading}(\boldsymbol{time}) = \boldsymbol{C} \times \Delta\boldsymbol{Pressure}(\boldsymbol{time}) \qquad \text{Equation 3}$$

Where “C” represents a constant that correlates pressure drop to mass loading, and is calibrated individually for each test. C is determined for each test by dividing the final mass on the filter by the final pressure drop, as is seen below in Equation 4.

$$C = \frac{\boldsymbol{Filter\ Mass\ Load}\ (t_{final})}{\Delta \boldsymbol{Pressure}(t_{final})} \qquad \text{Equation 4}$$

Ultimately this allows for an interpolation of the mass loading on the filter as a function of time using the pressure drop across the filter as the framework.

Using this method, real-time $PM_{2.5}$ emissions data from three cold start tests of the M5000 using the 3 stick fuel feeding approach was analyzed.

3.1.6 Baseline M5000 and G3300 Data

The baseline stove performance metrics for both stoves were based off of 3 replicate cold start water boil tests each, using 3 stick fuel feed rates. The pot skirt, stick spacing frame, and fuel feeding approach used in these tests were also used throughout all subsequent testing.

3.2 Results/Discussion - Baseline Stove Testing

3.2.1 Pot Skirt

The results of 6 tests with no pot skirt and 3 tests with a pot skirt can be seen below in Table 3.

Table 3. Pot Skirt's Effect on Stove Performance

Test Description	Cold Start with No Pot Skirt, M5000		Cold Start with Pot Skirt, M5000	
Number of Tests	6		3	
	Sample Mean	80% Confidence Interval	Sample Mean	80% Confidence Interval
Time to Boil (min)	36.9	36.1 - 37.8	30.5	30.2 - 30.9
Temperature Corrected Time to Boil (min)	37.3	36.4 - 38.2	30.0	29.4 - 30.5
Dry Fuel Consumed (g)	350	346 - 353	312	294 - 330
Char Produced (g)	25	24 - 25	21	19 - 23
Average FP (kW)	2.5	2.5 - 2.6	2.8	2.6 - 2.9
Total Thermal Efficiency (%)	29	29 - 30	35	34 - 36
PM (mg)	720	654 - 787	658	510 - 807
PM per Energy Delivered (mg/MJ_d)	440	400 - 480	370	280 - 470
CO (g/MJ_d)	3.3	3.0 - 3.7	3.3	3.1 - 3.6

T-test indicates no significant difference in the mean $PM_{2.5}$ emissions (p=0.24) or CO emissions (p=0.99), however a t-test indicates a significant difference in the means of the thermal efficiency with and without the pot skirt (p=0.01). The pot skirt increased the thermal efficiency by approximately 19%.

The pot skirt was designed to maintain a constant cross-sectional area between the chimney of the M5000 and the gap around the pot. This hypothetically minimizes the effect of the pot skirt on total draft through the stove, yet keeps the exhaust gases closer to the surface of the pot for a longer duration. The experimental results demonstrate that the pot skirt did increase thermal efficiency, but did not have a significant effect on emissions. This implies that the pot skirt did not significantly affect the processes within the combustion chamber that control emissions.

3.2.2 Stick Spacing

The results of the 3 cold start test using the stick spacing frame, and 3 cold start tests without the stick spacing frame can be seen below in Table 4. Both test sets include the pot skirt.

Table 4. Stick Spacing's Effect on Stove Performance

Test Description	Cold Start With Stick Spacing Frame on M5000		Cold Start Without stick spacing frame on M5000	
Number of Tests	3		3	
	Sample Mean	80% Confidence Interval	Sample Mean	80% Confidence Interval
Time to Boil (min)	28.9	27.0 - 30.9	30.5	30.2 - 30.9
Temperature Corrected Time to Boil (min)	28.7	26.8 - 30.5	30.0	29.4 - 30.5
Dry Fuel Consumed (g)	286	275 - 297	312	294 - 330
Char Produced (g)	17	15 - 18	21	19 - 23
Average FP (kW)	2.9	2.6 - 3.2	2.8	2.6 - 2.9
Total Thermal Efficiency (%)	36	35 - 37	35	34 - 36
PM (mg)	461	331 - 592	658	510 - 807
PM per Energy Delivered (mg/MJ_d)	280	190 - 360	370	280 - 470
CO (g/MJ_d)	2.7	2.6 - 2.8	3.3	3.1 - 3.6

Average PM emissions were 26% lower with the inclusion of a stick spacing frame, but not statistically significant (p=0.12). However, a statistically significant reduction in CO emissions (p=0.03) was observed with the inclusion of a stick spacing.

In regions where sticks are touching or nearly touching, it was observed that combustion may not occur. As pyrolysis gas is released from the fuel and enters regions of tight spacing, large fuel rich regions may be formed along the sides of the sticks. Fuel rich zones are known

contributors to Polycyclic Aromatic Hydrocarbon (PAH) formation and nucleation. Thus, it can be hypothesized that PM emissions are increased when stick spacing is reduced enough to prevent combustion from occuring between the fuel surfaces. It should be noted that for all subsequent testing the stick spacing frame was installed.

3.2.3 Firepower's Effect on Cold Start Water Boil Test Stove Performance

Firepower is a major variable of concern because it is largely defined by the fuel characteristics and the approach and diligence of the tester. Fuel characteristics were maintained constant throughout this study, thus this section focuses primarily on the potential range of effects on emissions, efficiency and time to boil due to variation in the tester's fuel feed rate. The results of 9 tests across a purposefully wide range of tester-defined firepowers, from 2.3 to 3.9 kW, are seen below in Table 5.

Table 5. Firepower's Effect on Stove Performance

Test Description	Cold Start With M5000, Varied Firepower		
Number of Tests	9		
	Sample Mean	80% Confidence Interval	Coefficient of Variation (COV)
Time to Boil (min)	27.6	25.3 - 29.9	0.18
Temperature Corrected Time to Boil (min)	27.4	25.2 - 29.6	0.18
Dry Fuel Consumed (g)	287	283 - 291	0.03
Char Produced (g)	20	19 – 22	0.17
Average FP (kW)	3.0	2.7 - 3.3	0.19
Total Thermal Efficiency (%)	36	35 - 37	0.04
PM (mg)	622	493 - 752	0.45
PM per Energy Delivered (mg/MJ_d)	380	300 – 460	0.46

Observation of the COV for $PM_{2.5}$ emissions compared to other variables led to the postulation that the $PM_{2.5}$ emissions are a strong function of firepower. A plot of $PM_{2.5}$ emissions as a function of firepower is seen below in Figure 9.

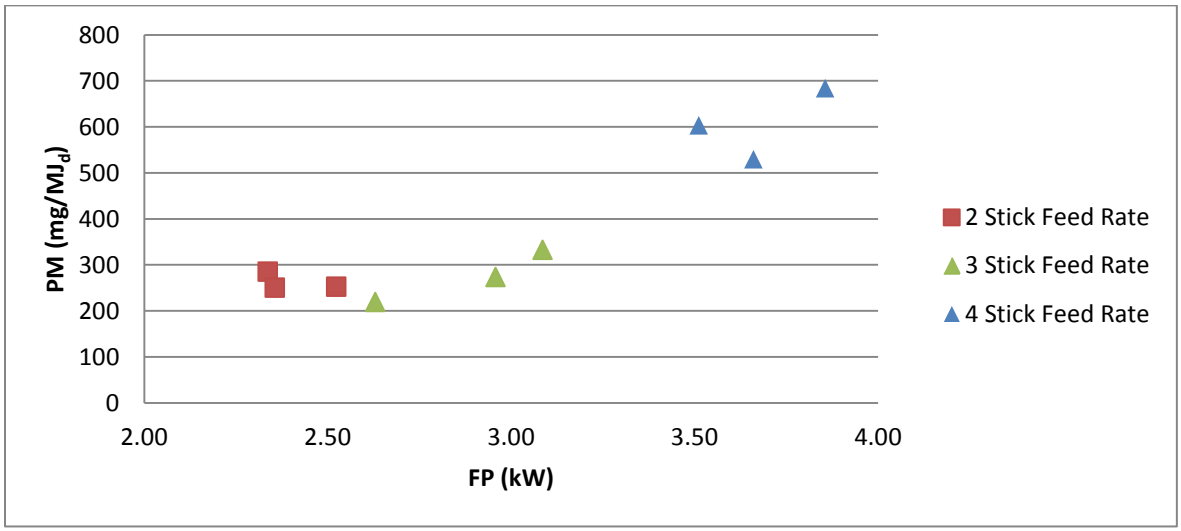

Figure 9. Firepower's Effect on PM Emissions

Figure 9 further confirms that PM emissions are a strong function of firepower. Additionally, the results of these tests indicate that the optimal firepower for minimizing PM emissions in the baseline M5000 is approximately 2.5 to 3 kW. Thus, for all subsequent tests, the three stick fuel feeding approach was utilized for the steady-state phase.

Plots of firepower versus time to boil and efficiency were also generated, and can be seen below in Figure 10 and Figure 11.

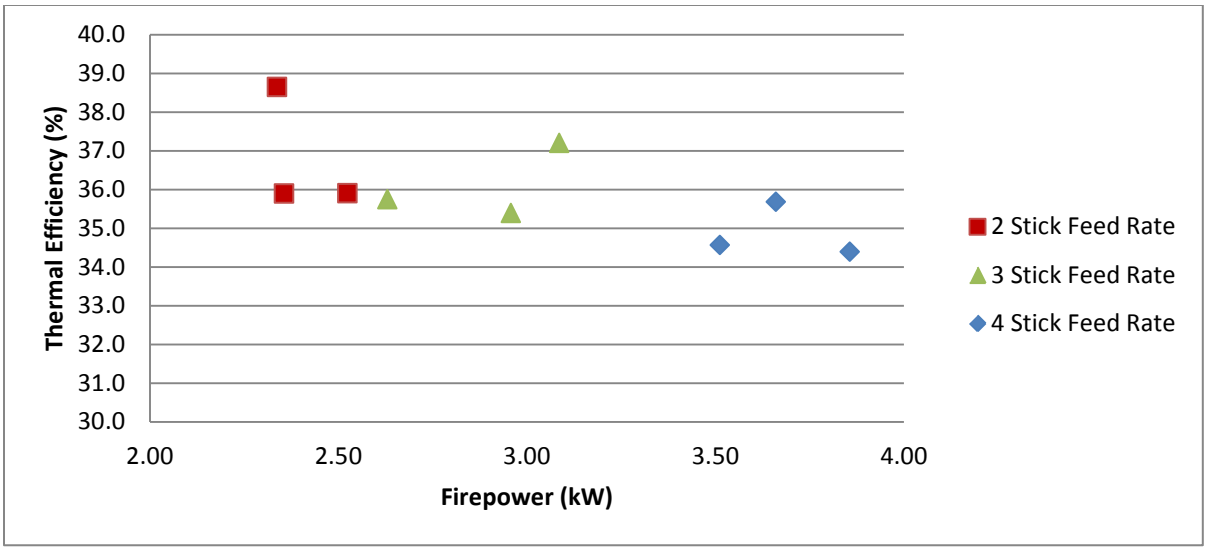

Figure 10. Relationship Between Thermal Efficiency and Firepower

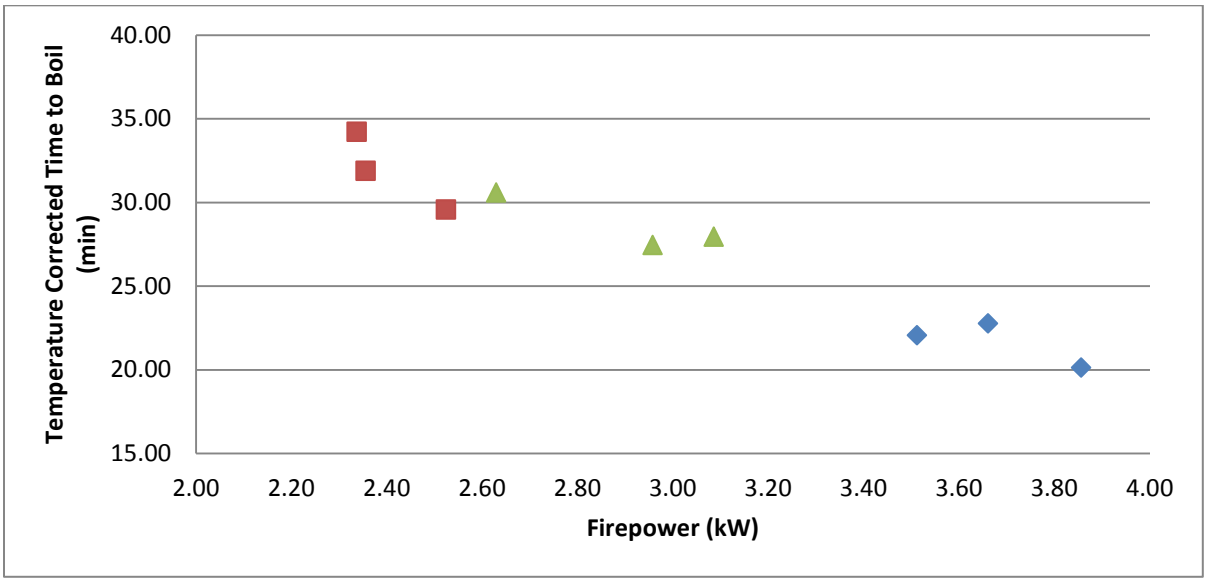

Figure 11. Relationship Between Time to Boil and Firepower

It can be seen that firepower appears to be strongly correlated to time to boil and weakly correlated to efficiency. This indicates that firepower must be a major consideration when gauging the performance of a stove. The subject of firepower's effect on stove performance is further explored in Sections 3.3 and 3.4.

3.2.4 Firepower's Effect on $PM_{2.5}$ emissions within a Cold Start Water Boil Test

Section 3.2.3 defined the effect of firepower on total emissions of $PM_{2.5}$ from a cold start water boil test, however understanding how the emissions rate changes within this a cold start test will prove useful for determining approaches to reduce the total emissions.

In section 3.2.3, we determined that the $PM_{2.5}$ emissions are a strong function of average cold start firepower. However, it is intrinsic that the firepower will change gradually throughout a water boil test. Figure 12 displays the carbon dioxide (CO_2) concentration sampled by the 5-gas analyzer throughout the duration of 3 cold start tests with the M5000, using the 3 stick feeding approach after burning of the shims. Assuming that nearly all of the carbon emitted from the stove is released as CO_2, a good assumption for rocket elbow wood burning cookstoves, we can use this CO_2 concentration as a convenient metric to gauge the real-time firepower.

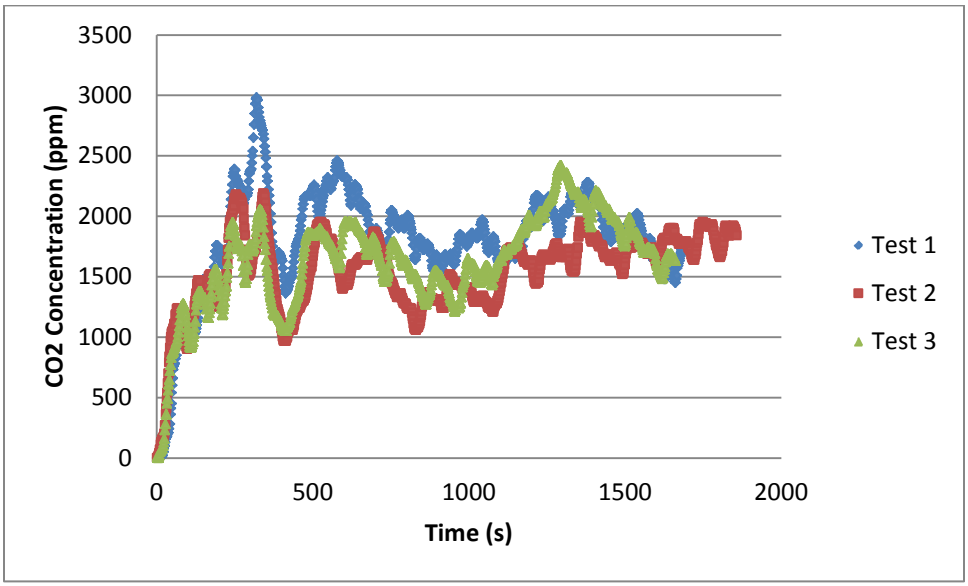

Figure 12. Real-Time CO2

It can be seen that the firepower gradually increases for approximately the first 400 seconds, while the shims are burning. It then drops off shortly around 500 seconds as the

transition from shims to 3 parallel sticks occurs. After the transition occurs the firepower appears to quickly reach a steady state.

The variation of firepower within the test implies that the $PM_{2.5}$ emissions rate will also change throughout the duration of a water boil test. In order to test this hypothesis, the real-time pressure drop data for each of these 3 tests was correlated to a cumulative $PM_{2.5}$ mass load on the gravimetric system's filter using the technique described in Section 3.1.4. The results of this analysis can be seen in Figure 13.

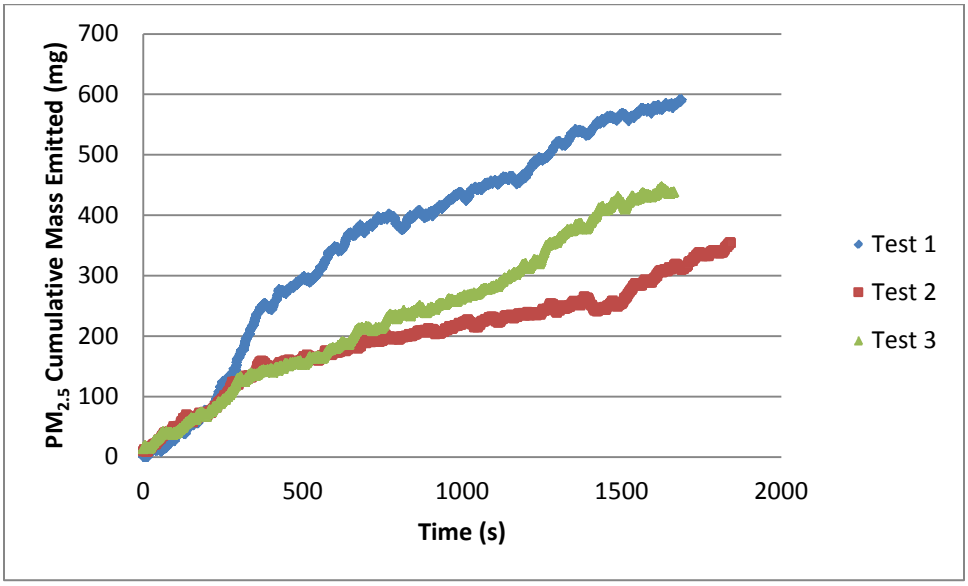

Figure 13. Real-Time Cumulative $PM_{2.5}$ Emissions for Cold Start Tests

It appears as though the mass loading on the filter tends to increase at a faster rate during the first 400 seconds of the test. Table 6 displays the percent of total PM emitted at 400 seconds to the percent of test time completed at 400 seconds.

Table 6. $PM_{2.5}$ Mass Emitted versus Time of Cold Start Test Completed

Test Name	1	2	3
Total PM Emitted (mg)	591	354	440
Total Time to Boil (s)	1688	1857	1662
Estimated Mass PM2.5 on Filter at 400 seconds (mg)	246	147	143
Percent of test time completed (%)	24%	22%	24%
Percent of total PM Emitted (%)	42%	42%	33%

The results in Table 6 confirm that the $PM_{2.5}$ emissions rate tends to be higher during the shim burning start-up phase than during the subsequent 3 stick burning portion of the test. For example, during test 1, at 400 seconds the test was 24% complete in terms of time, but 42% of the total mass of PM emitted during the test had already deposited on the filter. Additionally, the higher PM emissions rate observed during the start-up phase may imply that any variations to start-up could significantly affect the total measured PM2.5 emissions for a cold start. This demonstrates the importance of a highly consistent start-up procedure.

Using this data the cold start water-boil was split up into two phases in terms of $PM_{2.5}$ emissions: the “start-up” phase and the “steady-state” phase. The start-up phase lasts until the water temperature reaches approximately 30^{o} Celsius, when the shims are nearly consumed and the steady state phase lasts for the remainder of the test.

3.2.5 Baseline M5000

The baseline stove performance for the M5000 is detailed in Table 7. This data is based off of the 3 cold start tests using the 3 stick feeding approach with the pot skirt and stick spacing frame included. This data is used for comparison of performance improvements for the subsequent duration of this study. It can be seen that CO emissions are well within the IWA Tier 4 standard of 8 g/MJ.

Table 7. Baseline M5000 Performance

	Sample Mean	80% Confidence Interval	IWA Tier
Time to Boil (min)	28.9	27.0 - 30.9	N/A
Temperature Corrected Time to Boil (min)	28.7	26.8 – 30.5	N/A
Dry Fuel Consumed (g)	286	275 - 297	N/A
Char Produced (g)	17	15 - 18	N/A
Average FP (kW)	2.9	2.6 - 3.2	N/A
Total Thermal Efficiency (%)	36	35 - 37	Tier 3
PM (mg)	461	331 - 592	N/A
PM per Energy Delivered (mg/MJd)	280	210 - 340	Tier 2
CO (g/MJd)	2.7	2.6 - 2.8	Tier 4

3.2.6 Baseline G33000

The baseline stove performance for the G3300 is detailed in Table 8. This data is based off of the 3 cold start tests using the 3 stick feeding approach with the pot skirt and stick spacing frame included. This data is used for comparison of performance improvements for the subsequent duration of this study. It can also be seen that CO emissions are well within the IWA Tier 4 standard, however it should be noted the data for CO emissions is based on one sample.

Table 8. Baseline G3300 Performance

	Sample Mean	80% Confidence Interval	IWA Tier
Time to Boil (min)	24.1	21.9 - 26.3	N/A
Temperature Corrected Time to Boil (min)	24.0	21.8 - 26.3	N/A
Dry Fuel Consumed (g)	301	300 - 303	N/A
Char Produced (g)	21	20 - 22	N/A
Average FP (kW)	3.4	3.0 - 3.7	N/A
Total Thermal Efficiency (%)	34	33 - 34	Tier 2
PM (mg)	616	553 - 680	N/A
PM per Energy Delivered (mg/MJd)	380	340 - 420	Tier 2
CO (g/MJd)	3.4*	N/A	Tier 4

3.3 Experimental Correlation for baseline M5000 PM Emissions

The data garnered in Section 3.2 for the M5000 stove with a pot skirt and stick spacing frame were used to generate an experimental correlation for baseline $PM_{2.5}$ emissions. The desired output of the model is $PM_{2.5}$ emissions per Mega joule delivered to the water. It was initially hypothesized that the output was a function of the independent variables firepower, time to boil and efficiency. However, Figure 11, a plot of time to boil versus firepower, indicated that firepower and time to boil are strongly correlated. Thus including both firepower and time to boil as inputs is unnecessary. Figure 14, a plot of $PM_{2.5}$ emissions versus efficiency does not show any strong correlation. Additionally, when considering how efficiency changes from approximately 34.4% to 38.6% across the range of tests, whereas firepower ranges from 2.3 kW to 3.9 kW, it can be seen that the predicted emissions will be highly sensitive to minor variations in the efficiency input, leading to potentially large errors.

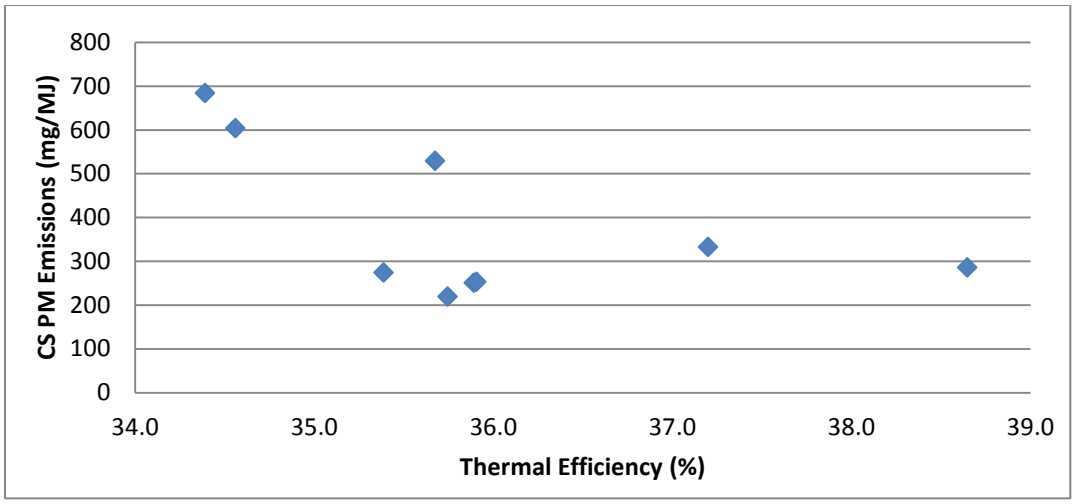

Figure 14. $PM_{2.5}$ Emissions as a Function of Thermal Efficiency

Thus it was concluded that the PM emissions for the baseline M5000 would be correlated only to the firepower. Figure 15 displays a second order polynomial trendline to the PM versus firepower curve, derived using Microsoft Excel.

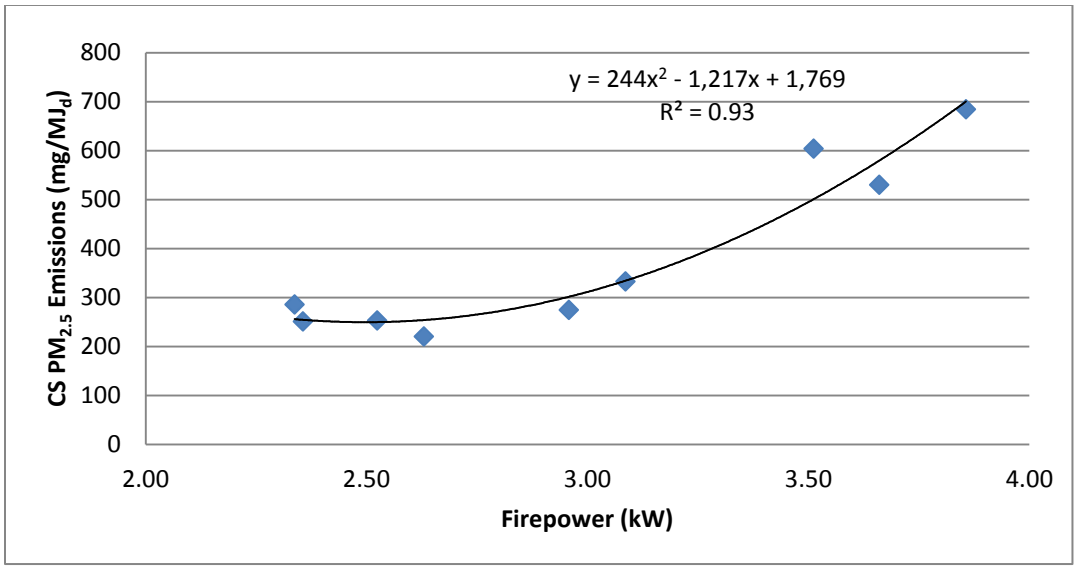

Figure 15. $PM_{2.5}$ Emissions Model for M5000 Cold Start Tests

The equation for $PM_{2.5}$ emissions as a function of firepower can be seen below in Equation 5.

$$\frac{PM_{2.5}}{MJ_d} = 244 \cdot FP^2 - 1217 \cdot FP + 1769$$ Equation 5

The R^2 value for this correlation is 0.93, indicating a good fit for the experimental model to the data. This correlation is used again in Section 5 to aid in the understanding of the effect of firepower variations induced by forced draft on emissions. It should be noted that this model is only intended to be accurate for M5000 cold start $PM_{2.5}$ emissions with a pot skirt and stick spacing frame in place, within a firepower range of 2.3 to 3.9 kW.

Additional data regarding the relationship between $PM_{2.5}$ emissions and firepower has been documented in literature. In Figure 16, a similar trend between a PM emissions and firepower in a rocket elbow stove is seen [12]. It should be noted that the first two plots listed in the legend are generated from test data where a pot was not on the stove, and may not be applicable. The similar relationship reaffirms the validity of the firepower and PM2.5 emissions relationship observed during the testing of the M5000, and helps to justify the use of an experimental correlation.

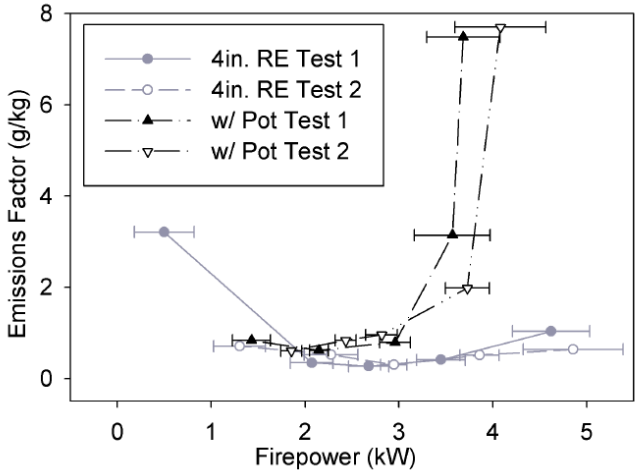

Figure 16. PM emissions and Firepower Relationship documented in literature [12]

3.4 Firepower Corrected PM Emissions

In the previous sections, it was found that $PM_{2.5}$ emissions are related to the square of firepower, and a model for emissions was derived that is only applicable to the M5000. The inference that $PM_{2.5}$ emissions are a strong function of firepower can be logically extended to most, if not all, biomass cookstoves. This indicates that firepower must be a major consideration when gauging the performance of a stove. For example, consider a situation in which a tester is trying to compare $PM_{2.5}$ emissions between Stove A and Stove B, both of which are designed to be operated at 3 kW. The tester attempts to maintain a consistent firepower between tests of both stoves to the best of their abilities, however the average firepower for tests of Stove A turns out to be 3 kW, while the average firepower for tests of Stove B turns out to be 3.5 kW. Considering the squared relationship between $PM_{2.5}$ and firepower seen in Figure 15 and Equation 5, then it is clearly not fair to compare the emissions from these stoves.

One potential solution to this problem is to ensure that firepower is maintained constant with as great precision as possible. For example, a tester may watch real-time CO_2 emissions and adjust their fuel feed rate accordingly, ensuring that the average firepower is maintained constant among tests. However, for charcoal stoves or top loading stoves, this method is not practical as it is difficult to adjust the fuel feed rate with precision.

Another potential solution to this problem is to devise a method to correct the $PM_{2.5}$ emissions for variations in the firepower. Benefits of this method may include more accurate comparison of stoves that were tested at different firepowers, a reduction in the spread of $PM_{2.5}$ emissions data among tests of the same stove by taking firepower out of the equation, and a better understanding of what additional variables may be causing spread in the $PM_{2.5}$ data.

One way to correct $PM_{2.5}$ emissions for firepower variations is through the use of a function, $PM_{2.5}$ = function(Firepower), that is stove specific. For example, consider again the scenario in

which both Stove A and Stove B are designed to run at 3 kW, but where Stove B was incidentally run at 3.5 kW. If we know that PM emissions are a strong function of firepower, and if we know the general function, $PM_{2.5}$ = function(Firepower), for Stove B, then we can correct the Stove B emissions data from 3.5 kW to 3.0 kW by subtracting the expected increase in emissions resulting from the increase in 0.5kW of firepower. Equation 6 and Equation 7 provide the details behind this method.

$$\boldsymbol{PM_{corrected} = PM_{measured} - Error} \qquad \text{Equation 6}$$

Where the error is defined by stove specific functions of $PM_{2.5}$ based on firepower.

$$\boldsymbol{Error = PM(FP_{Measured}) - PM\ (FP_{Corrected})} \qquad \text{Equation 7}$$

Figure 17 provides a graphical description of the method, where the distance labeled error is the error in PM emissions associated with the firepower variation from $FP_{corrected}$ to $FP_{measured}$ and the function $PM_{2.5}$ = function(Firepower) is the stove specific function.

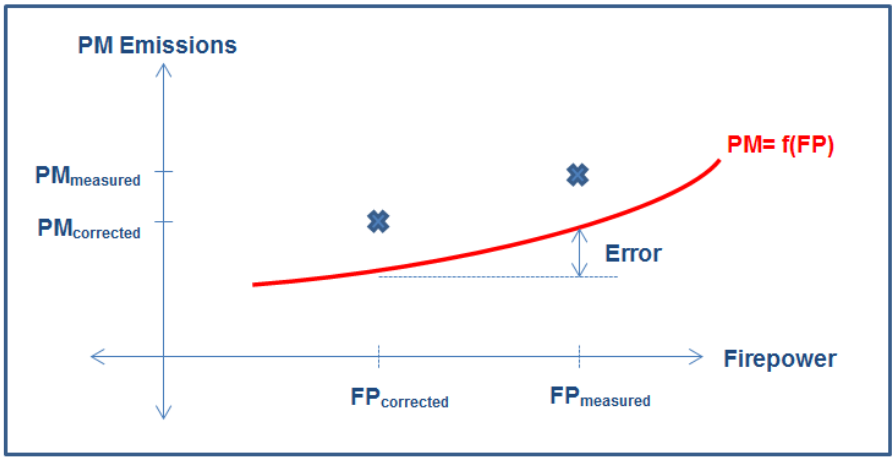

Figure 17. Firepower Corrected $PM_{2.5}$ Emissions

In the aforementioned hypothetical scenario, where the $PM_{2.5}$ from Stove B will be corrected for better comparison with Stove A, the measured firepower would be 3.5kW and the corrected firepower would be 3.0 kW. The function for $PM_{2.5}$ of firepower found in the error equation

would be stove specific. For example, if Stove B was the M5000 then the Error equation may be:

$$Error = \left(244 \cdot {FP_{Measured}}^2 - 1217 \cdot FP_{Measured} + 1769\right) - \left(244 \cdot {FP_{Corrected}}^2 - 1217 \cdot FP_{Corrected} + 1769\right)$$

An advantage of this method is that one only needs to derive a stove specific $PM_{2.5}$ function for one of the stove in which the comparison is desired. However, deriving the stove specific $PM_{2.5}$ functions for both stoves and overlaying their plots can provide insight into which firepower regions the stoves operate best in and/or outperform the other stove in. It can be conjectured that this method could also help standardizing results. For example, the high power $PM_{2.5}$ emissions for all family size rocket elbow stoves could be standardized to 3 kW for better and fairer comparison between stoves.

The obvious disadvantage of this method is that an equation for $PM_{2.5}$ as a function of firepower must be derived for any stove in which firepower corrected $PM_{2.5}$ data is desired. Additionally, a potentially major disadvantage of this method is that the testing necessary for the derivation of the stove specific equation must be done in a highly controlled environment where it is certain that $PM_{2.5}$ is only a function of firepower. Error associated with this method can be directly correlated to errors in the derivation of the stove specific $PM_{2.5}$ function. If this is not considered properly than this method can produce misleading results.

Another potential solution is to derive a general function for $PM_{2.5}$ emissions that can be applied to all forms of biomass combustion. In this study, we found that $PM_{2.5}$ a very strong function of firepower. However throughout the duration of the study we keep the fuel and stove characteristics constant. Consequently, a general function for $PM_{2.5}$ might then include inputs of firepower, fuel type, fuel density and excess air ratio. It should also be noted that, this function would have to output mass of emissions, instead of mass of emissions per energy delivered as is used in this study. Including the energy delivered term would prevent the function from

applying to general $PM_{2.5}$ emissions from biomass combustion across a range of different sized stoves.

A general model for $PM_{2.5}$ from biomass combustion would allow for an increased understanding of the variability associated with $PM_{2.5}$ emissions, improved designs for emissions reductions, potential improvements in stove modeling, and fair comparisons to be made between stoves. However, derivation of this function would require extensive experimentation and is beyond the scope of this study.

4 EGR – Experimental Optimization for PM emissions reductions

The idea of an exhaust gas recirculation (EGR) cookstove was produced from the CSU cookstoves laboratory in 2012. Exhaust gas recirculation is a concept that is primarily applied to Internal Combustion Engines to reduce NOx emissions, sometimes at the cost of increased particulate emissions. Surprisingly, early studies confirmed that recirculating the exhaust gas in a cookstove reduced the total mass of particulate matter emitted. Pictured below is the setup used for initial testing of exhaust gas recirculation.

Figure 18: Early EGR Testing Platform

With promising preliminary results, a Department of Energy grant was received that made further exploration of exhaust gas recirculation possible. The following section describes the experimental optimization work on the EGR stove. The goal of this optimization work was to achieve significant a significant reduction in $PM_{2.5}$ emissions through the application of EGR to the M5000.

4.1 Testing Platform

In order to ensure thorough optimization of the EGR stove, a testing platform was designed that allowed for manipulation of the key variables that affect emissions performance. The EGR stove testing platform concept is pictured in Figure 19 (a) and Figure 19 (b).

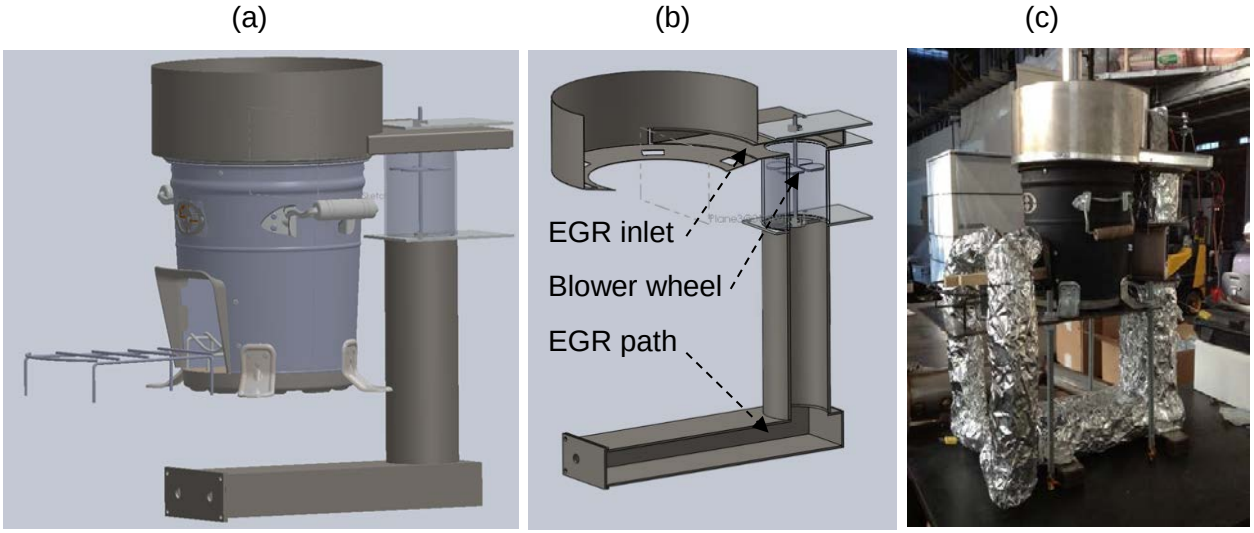

Figure 19. a) EGR Stove Concept Drawing, b) Cross-sectional View, c) EGR Stove

The base cookstove for the EGR stove testing platform is the Envirofit M5000, seen in Figure 19 (a) and Figure 19 (c). A blower wheel, seen in Figure 19 (a) and Figure 19 (b), draws exhaust gas through a port in the pot skirt. The exhaust gas is then pushed towards the mouth of the combustion chamber through the EGR path. Note that a portion of the conduit that directs the recirculated gas back into the mouth of the combustion chamber is not pictured in the concept drawings. The complete testing platform is seen in Figure 19 (c). In the completed testing platform, a pulse width modulator and power supply were used to control the speed of the motor that powers the squirrel cage fan. Additionally, a Thermal-Electric Generator was incorporated along the EGR path in order to characterize the potential for power recovery from the hot exhaust gas.

4.2 Key Variables

There are many variables that affect cookstove $PM_{2.5}$ emissions. General knowledge of PM formation and growth/oxidation allows one to generate some key variables concerning how EGR is applied to a cookstove. These variables are listed below.

- Temperature of recirculated exhaust gas
- Exhaust gas composition
- Exhaust gas injection location and nozzle configuration
- Exhaust gas recirculation flow rate

The effect of these key variables on stove performance was determined through experimentation.

4.3 Testing Methodology

4.3.1 Recirculated Gas Composition

To ensure that no ambient air was being drawn into the EGR pot skirt inlet, two sets of WBTs were run with consistent EGR flow rates, injection locations and nozzle configurations, but with different EGR inlet setups. The first test set utilized the normal EGR pot skirt inlet set up. In the second set, a conduit was routed from the normal EGR pot skirt inlet to the chimney of the M5000, seen in Figure 20.

Figure 20. Conduit Routed from Stove Chimney to EGR Path

The conduit ensured that only exhaust gas was being drawn in to the EGR Path. The concentration of molecular oxygen was then sampled throughout the tests at the midpoint of the EGR path using the Testo gas analyzer. Comparison of the concentrations of oxygen between the two test sets then indicated if ambient air was intruding into the recirculated exhaust gas at high flow rates.

4.3.2 Temperature of Recirculated Gas

The temperature of the recirculated exhaust gas was tested by incorporating a heater tape with PID temperature control into the testing platform. The setup for testing of this variable can be seen in Figure 21.

Figure 21. Recirculated Exhaust Gas Temperature Testing Platform

A set of 10 cold start WBTs was completed, in which all variables were held constant except for the recirculated gas temperature. The average recirculated gas temperature was varied from approximately 20^{o}C to 100^{o}C. The lower bound of tested temperatures replicated the effect of exhaust gas that had been entirely cooled to ambient temperatures. The upper bound of tested temperatures represented a scenario in which the exhaust gas temperatures at the lower edge of the pot were maintained nearly constant until reinjection in to the combustion chamber. The temperature was controlled through the use of an ice bath on the lower bound of tested temperatures and an electrical resistance heater tape for the other tested temperatures. Thermocouples along the EGR path were used to measure temperature of the exhaust gas at one second intervals.

4.3.3 Nozzle and Flow Rate Optimization procedure

It can easily be postulated that there are innumerable methods by which the exhaust gas can be injected into the combustion chamber, where injection methods are some combination of the key parameters: nozzle geometry, nozzle location and flow rate. Considering how

emissions can be a strong function of any of these key parameters, fair comparison of different injection methods can be a difficult task. The approach used in this study was to compare the minimized $PM_{2.5}$ emissions for each nozzle configuration.

As a result of initial difficulties with achieving emissions reductions, a unique nozzle and flow rate optimization procedure was developed. This procedure determines the crudely minimized $PM_{2.5}$ emissions for a particular nozzle configuration in a highly time efficiency manner, and relies on two assumptions that sacrifice minor accuracy. These assumptions include the two firepower phase assumption and the constant efficiency during steady state assumption, and will be discussed in further detail below. The flow chart seen in Figure 22 illustrates the general progression of the test procedure.

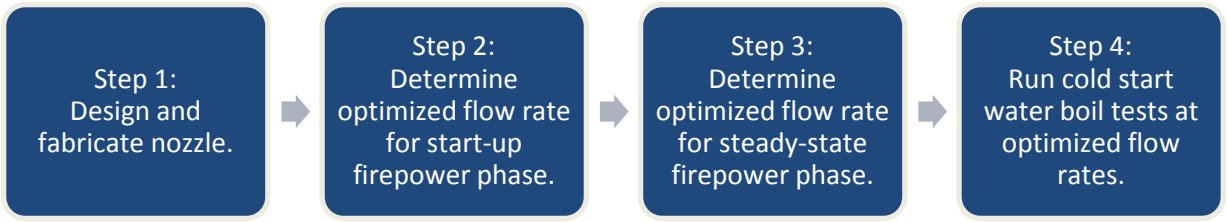

Figure 22. Nozzle/Flow Rate Optimization Procedure

In the EGR Experimental Optimization portion of this study, 3 iterations of this procedure were completed. The exact details of each step in a sample iteration of the procedure are discussed below.

Step 1: A nozzle is designed and fabricated. The nozzle is designed using a combination of fluid mechanics and combustion concepts and previous experimental results.

Step 2: In step 2 the optimized flow rate for $PM_{2.5}$ emissions reductions for the start-up phase is determined. For each data point, the standard cold-start water boil test procedure was followed but was concluded at a water temperature of 30 ^{o}C. A water temperature of 30^{o}C was

selected to be the ending value for these tests. When the water temperature reaches 30°C the firepower is no longer in a transient phase and has entered a steady state. The flow rate was altered at 10 to 20 SLPM intervals, with 1 to 2 data points collected per flow rate. Sample results of a start-up phase flow rate optimization can be seen in Figure 23. It can be seen that the optimized start-up phase flow rate for this example data set is approximately 40 SLPM.

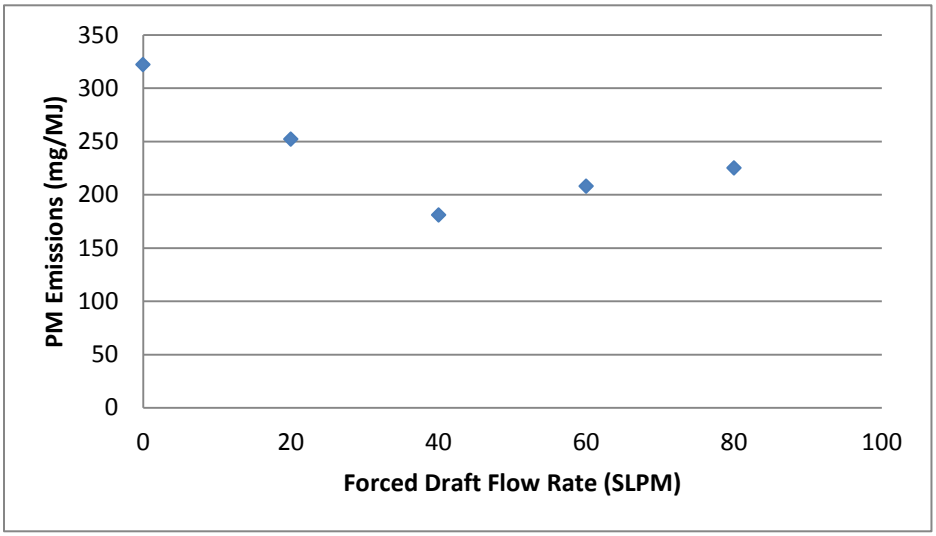

Figure 23. Example Start-up Phase Flow Rate Optimization

Step 3: In step 3, the optimized flow rate for $PM_{2.5}$ emissions reductions for the steady state firepower phase was determined. A quasi-simmer test approach was utilized for the determination of the steady state optimized flow rate. Firstly, the stove body, pot and water were brought up to simmer temperatures. Once steady state simmer temperatures were achieved, the charcoal and burning fuel were removed and the pot and water were left in place. A known weight of fuel was then reignited in the combustion chamber with a propane torch. A propane torch was necessary to reignite the fuel because the steady state firepower phase (3 - ¾" x ¾" x 12" pine sticks) fuel feeding approach was used from the start of each sample. The fire was allowed to burn for one minute before sampling of $PM_{2.5}$ began. This preventedsampling $PM_{2.5}$ produced during the ignition of the sticks. The $PM_{2.5}$ emissions were then sampled for ten minutes, or until the sticks were nearly consumed, while the firepower was

held at a constant level. Upon completion of the $PM_{2.5}$ sampling period the leftover fuel and charcoal were removed and weighed. The re-ignition process and subsequent ten minute sampling period was then repeated, but at an altered flow rate. Throughout the process of this test the water and pot remained in place at boiling temperatures. Additionally, the time between sampling periods never exceeded 3 minutes, preventing any significant cooling of the stove or pot. This test procedure allowed for a crude relationship to be developed between PM emissions and flow rate for a particular nozzle setup during the steady-state firepower phase. The PM emissions were characterized in terms of mass of $PM_{2.5}$ emitted per mass of fuel consumed, referred to as the Emissions Factor (EF). In the calculation of the EF, the weight of fuel consumed was corrected for moisture content and for sample time. Example results of a steady-state firepower phase flow rate optimization can be seen in Figure 24. It can be seen that the example optimized steady-state phase flow rate is approximately 80 SLPM.

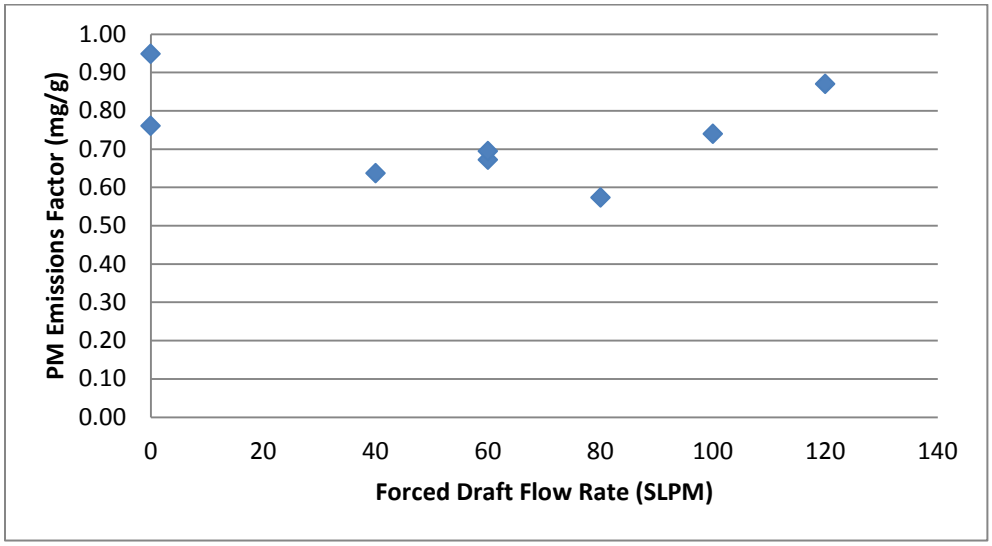

Figure 24. Example Steady-State Phase Flow Rate Optimization

Step 4: In step 4, the minimized PM emissions for a particular nozzle were determined. Using the optimized flow rates determined in Steps 2 and 3, cold start water boil tests were completed. The optimized flow rate determined in step 2 would be used until a water temperature of about 30° Celsius and the optimized flow rate determined in step 3 would be

used for the remaining time of the cold start. If it is not clear what the true optimized flow rates are, then several water boil test should be run at each of the potential optimized flow rates. The PM emissions resulting from step 4, along with supplementary conclusions derived from steps 2 and 3, were then used in the design of the next nozzle.

Assumptions: In this optimization procedure, the cold start water boil test is split in to two phases, the start-up phase and the steady-state phase. In Section 3.2.4, entitled "Firepower's Effect on $PM_{2.5}$ Emissions within a Cold Start Water Boil Test", it was concluded that emissions during the start-up phase, where there is a more transient and generally lower firepower, and the emissions during the steady state firepower phase, where there is a steady and generally higher firepower, are different. Thus, it was hypothesized that different firepowers will require different forced draft flow rates to achieve maximal PM emissions reductions. Consequently, the cold start WBT emissions will be perfectly minimized if the flow rate tracks the real-time firepower. For the flow rate to follow the real-time firepower continuously, a function relating firepower and flow rate would have to be developed, requiring the determination of optimized flow rates for numerous firepowers, and a control system would have to be developed in which the firepower is continuously monitored. This would require a major time investment for each nozzle configuration.

In order to save time, optimized flow rates were determined for only two distinct firepower phases and the flow rates during the cold start tests followed a step function pattern. The assumption inherent in this method is that the measured $PM_{2.5}$ emissions for a cold start test using the two firepower phase model will be similar to emissions from a cold start test in which the flow rate continuously follows real-time firepower.

Additionally, the validity of the optimized forced draft flow rate determined by the steady-state flow rate optimization procedure relies on the assumption that the forced draft flow rate does not significantly affect the thermal efficiency of the stove during the steady state firepower

phase. This assumption was necessary because it was not practical to take accurate measurements of the energy delivered to the water during this test.

Nozzles Tested: Ultimately, three iterations of this optimization procedure were completed for the EGR stove. The three different nozzle configurations that were tested are seen in Figure 25.

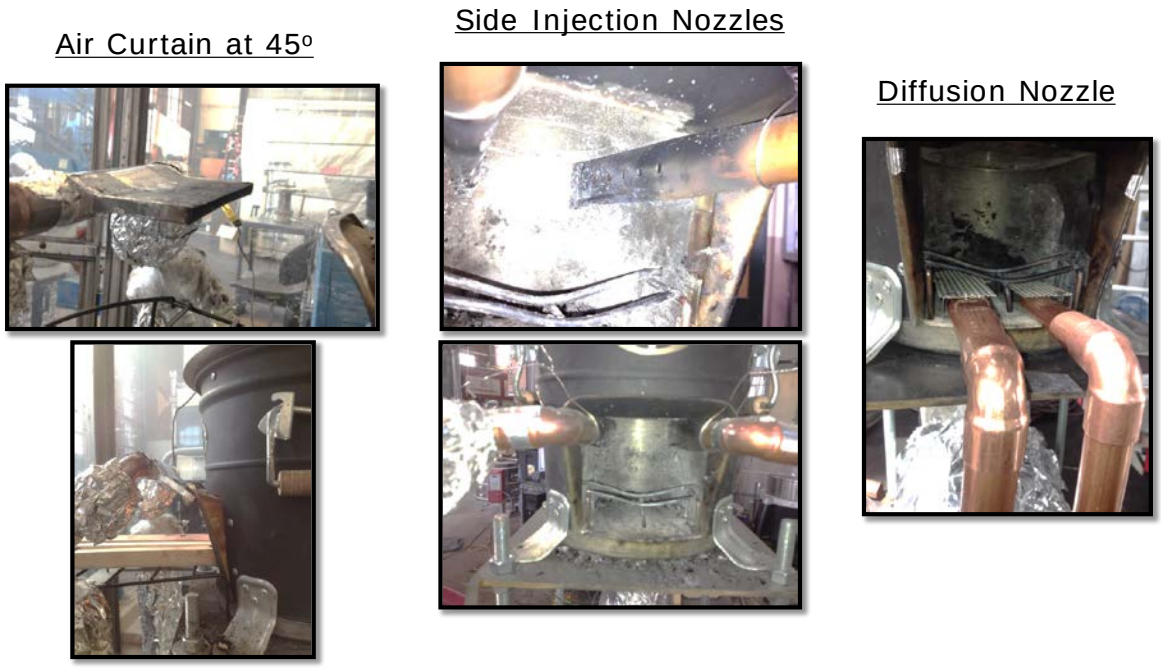

Figure 25. EGR Stove Nozzles

These setups occupy two major injection locations. The approximate injection locations are displayed below in a cross-sectional depiction of the M5000.

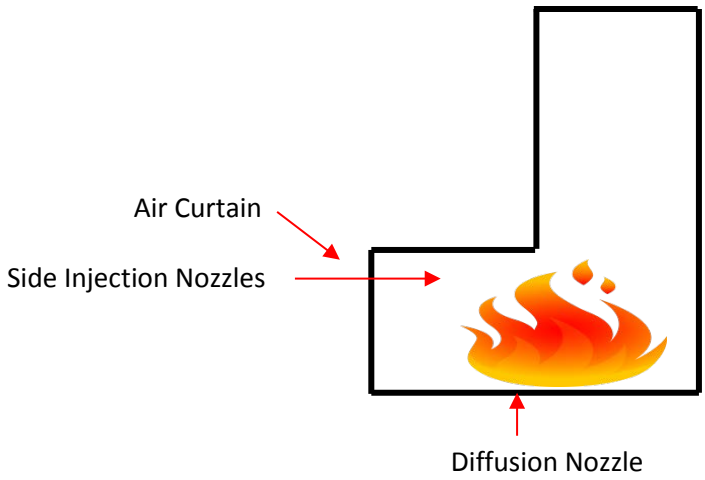

Figure 26. EGR Stove Nozzle Injection Locations

The diffusion nozzle injects below the charcoal bed and the Air Curtain and the Side Injection Nozzles inject near the top of the combustion chamber. The air curtain has approximately a 4"x1/4" gap and injects downwards at an angle of 45^{o} from horizontal. The side injection nozzles have 4.9 millimeter diameter holes that inject air perpendicularly to the natural draft of the stove. The diffusion nozzle uses two ¾' diameter pipes that are flattened and direct air beneath a perforated metal grate.

4.4 Results/Discussion

4.4.1 Recirculated Gas Composition

The composition of the recirculated gas can have a significant effect on the concentrations of nitrogen, oxygen, carbon dioxide and carbon monoxide within the combustion chamber. At high EGR flow rates, it may be possible that ambient air is being drawn into the EGR pot skirt inlet. This could significantly affect the composition of the recirculated gas and contribute to error among tests, especially when attempting to isolate the effect of varying the EGR flow rate. In order to ensure that no ambient air was mixed with the recirculated exhaust gas throughout the experimental optimization, two sets of cold start WBTs were completed. For one set the

normal testing platform was used, while for the other set a conduit (referred to as the modified EGR inlet in Table 9) was routed from the normal EGR pot skirt inlet to the chimney of the M5000. This modified EGR inlet ensured that the recirculated gas was composed completely of exhaust gas. For all tests, EGR flow rates were kept consistent and the Air Curtain nozzle setup was used. The molecular oxygen concentration was sampled throughout the tests midway through the recirculated exhaust gas path. The results of these tests can be seen in Table 9.

Table 9. Recirculated Exhaust Gas Composition

Test Number	Testing Platform	Average O2 Concentration in Recirculated Gas (%)	PM Emissions (mg/MJd)
1	Standard	15.9	260
2	Standard	16.1	390
3	Modified EGR inlet	16.4	320
4	Modified EGR inlet	16.9	250

It can be seen that the average oxygen concentration in the recirculated exhaust gas appears to increase slightly when the modified EGR inlet is installed. However, if ambient air was being drawn in to the standard EGR pot skirt inlet, then the oxygen concentration in the recirculated exhaust gas would be expected to decrease when the modified EGR inlet is installed. This effect was not observed, indicating that no ambient air is drawn into the standard EGR inlet at high EGR flow rates. The fact that the opposite relationship is observed may instead indicate that when the modified EGR inlet is installed, the gas is drawn in before combustion is complete.

4.4.2 Temperature of Recirculated Gas

The effect of temperature of the recirculated gas was tested through a set of eight cold start WBTs. Four different gas path setpoint temperatures were tested, with two replicates for each temperature. The results of these tests are pictured in Figure 27. The temperature value plotted on the x-axis represents the average measured temperature of the gas throughout a WBT, measured immediately before injection into the combustion chamber. It should be noted that for all tests, the Air Curtain style nozzle was used, and the EGR flow rates were kept consistently at approximately 70 SLPM.

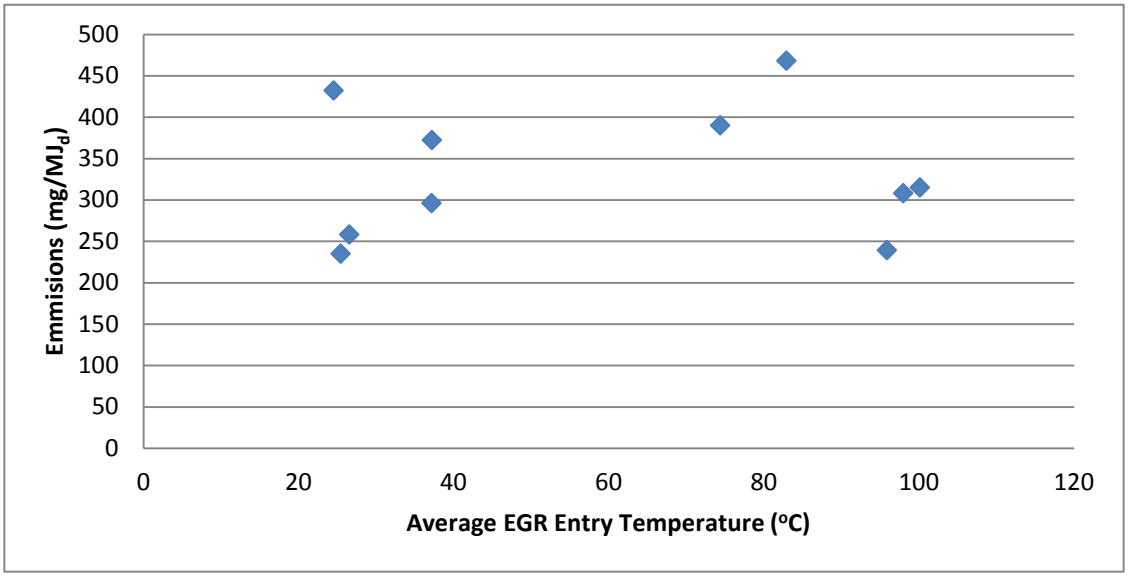

Figure 27. Recirculated Exhaust Gas Temperature Testing Results

Observation of the results of this study concludes that no strong correlation exists between practical gas path temperature variation and PM emissions. Thus for all further testing, insulation along the EGR path was not incorporated into the testing platform.

4.4.3 Nozzle and Flow Rate Optimization

Results of crude flow rate optimizations for the air curtain, diffusion and side injection nozzle are displayed in Figure 28, Figure 29 and Figure 30.

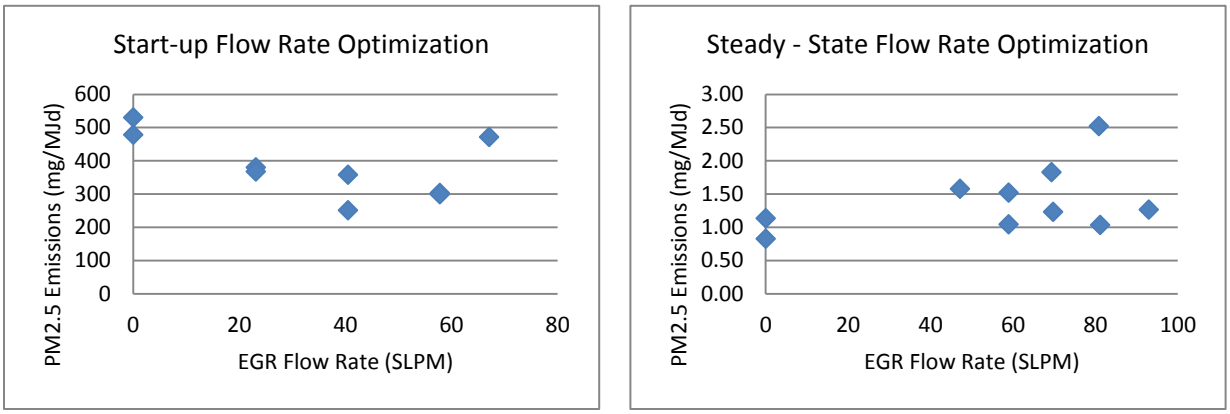

Figure 28. Air Curtain Nozzle EGR Flow Rate Optimization

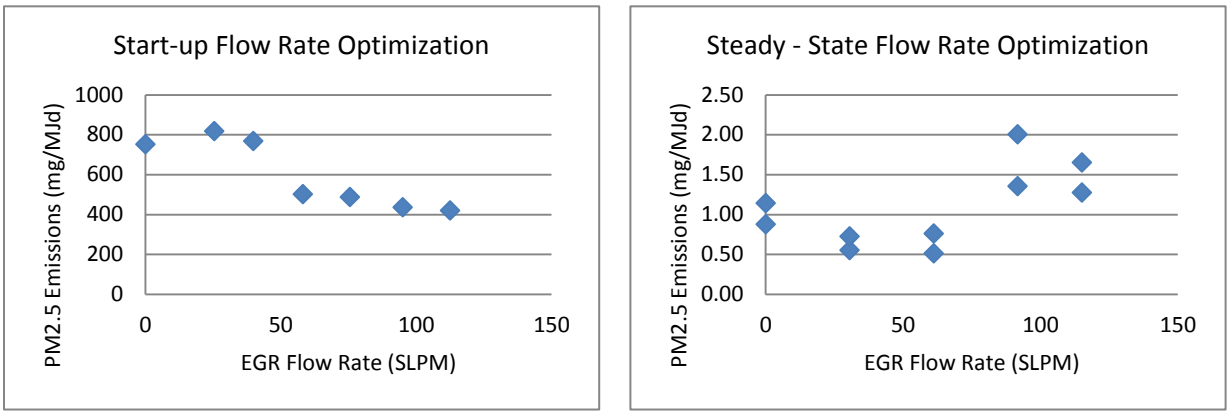

Figure 29. Diffusion Nozzle EGR Flow Rate Optimization

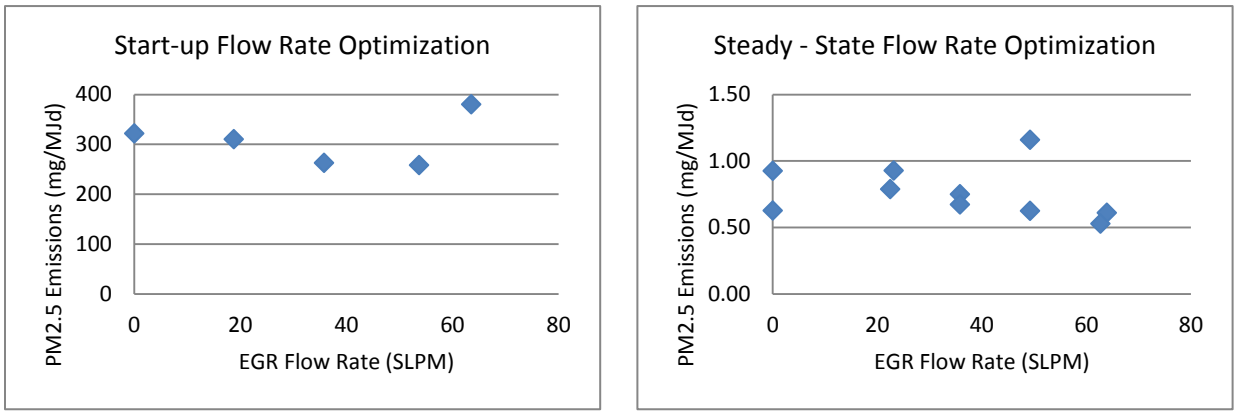

Figure 30. Side Injection Nozzles EGR Flow Rate Optimization

Table 10 summarizes the major results of the flow rate optimizations. The values for the optimized flow rate were determined by selecting the approximate minimum location on the plots in Figure 28 through Figure 30. The values for $PM_{2.5}$ emissions in Table 10 represent the phase specific emissions at the optimized EGR flow rates.

Table 10. EGR Nozzle Flow Rate Optimization

Phase	Nozzle Set Up	Diffusion Nozzle	Air Curtain	Side Injection Nozzles
Start-up	Optimized Flow (SLPM)	110	40	50
	PM (mg/MJ_d)	420	310	260
	PM Emissions Factor (mg/g)	2.2	1.3	1.1
Steady-State	Optimized Flow (SLPM)	60	0	70
	PM Emission Factor (mg/g)	0.64	0.98	0.57

Using the optimized flow rates seen in Table 10, cold start WBTs were completed for each nozzle configuration. The results of these tests can be seen in Table 11. The $PM_{2.5}$ emissions for these tests represent the nearly minimized $PM_{2.5}$ emissions for each nozzle configuration. It can be seen in Table 11 that the Side Injection Nozzles, with injection near the top of the

combustion chamber, led to the greatest reduction in $PM_{2.5}$ emissions, with a 44% reduction from the baseline M5000 $PM_{2.5}$ emissions found in Section 3.2.5. However, the sample size is too small to draw a statistically significant conclusion. It also should be noted that the side injection nozzles appear to increase the firepower, compared to typical baseline firepower and the other two nozzle configuration's firepower.

Table 11. Minimized $PM_{2.5}$ Emissions for Various Nozzles Using EGR

Nozzle Type	Air Curtain	Diffusion	Side Injection
Number of Tests	1	1	2
Time to Boil (min)	32.4	40.8	28.9
Temperature Corrected Time to Boil (min)	32.1	40.2	32.1
Dry Fuel Consumed (g)	280	282	317
Average FP (kW)	2.4	2.0	2.9
Total Thermal Efficiency (%)	36	35	32
PM (mg)	294	334	248
PM per Energy Delivered (mg/MJd)	180	200	150
CO (g/MJd)	-	-	2.7*

*CO emissions based off of one test

Using the emissions factors found in Table 10, and with knowledge of the total amount of fuel consumed in a WBT, the total weight of emitted PM can be predicted. Comparison between the predicted PM and measured PM allows one to conclude whether the measurements in the flow rate optimization tests can provide an accurate representation for emissions from a full cold start WBT. The comparison between predicted and measured PM emissions can be seen in Table 12.

Table 12. Predicted versus Measured $PM_{2.5}$ Emissions

Nozzle Setup	Diffusion Nozzle	Air Curtain	Side Injection Nozzles
Total Dry Weight Fuel Use to Boil (g)	282	280	317
Dry Weight Fuel Use in Start-up Phase (g)	66	75	80
Dry Weight Fuel Use in Steady-state Phase (g)	220	210	240
Predicted PM Start-up Phase (mg)	147	101	90
Predicted PM Steady-state Phase (mg)	138	185	135
Total Predicted PM (mg)	285	286	225
Measured PM (mg)	334	294	248
Error (%)	14.6%	2.9%	9.3%

The error values seen in Table 12 indicate that the shorter tests used in the flow rate optimization can be used as predictors of the total optimized cold start emissions with accuracy. Additionally, this indicates that the constant efficiency assumption in step 3 of the nozzle optimization procedure does not induce a significant inaccuracy.

Ultimately, the results of this section indicate that an emissions reduction can be achieved through the application of EGR to the M5000 through the side injection nozzles, and confirms the validity of the optimization procedures.

5 Understanding EGR emissions reductions mechanisms

In Section 4, it was shown that a significant emissions reduction can be achieved through the application of EGR. In section 5 we isolate and measure the driving mechanisms behind the emissions reduction observed with EGR through the side injection nozzles.

5.1 Testing Platform

The M5000 was used for these tests, however, the EGR stove testing platform was modified. Conduit was routed such that gas could be injected into the M5000 from compressed gas cylinders. The flow rate of the injected gases was regulated through a high performance Alicat Mass Flow Controller.

5.2 Testing Methodology

It was hypothesized that the reduction in PM emissions with the EGR cookstove could be the net result of a combination of the following mechanisms:

- Increased particle residence time
- Chemical Effects of O_2/CO_2
- Mixing
- Dilution
- Temperature
- Firepower

Tests were completed in order to isolate, as best as possible, the relative magnitude of each of these mechanisms with reference to the EGR side injection nozzles configuration.

5.2.1 Increased Particle Residence Time

The effect of increased residence time of particulate in the flame was isolated by injecting a particulate-free replicate EGR gas into the stove. The EGR replicate gas was composed of 15% O_2, 5% CO_2 and 80% N_2, similar to the measured composition in Section 4.4.1. The gas was injected at an equivalent mass flow rate to the optimized mass flow rates used for the Side Injection Nozzles. In Section 4.4.3, it was determined that the optimized flow rates for the Side Injection Nozzles are 50 to 70 SLPM for the start-up and steady-state firepower phases, respectively. However, measurement of the temperature at the blower wheel throughout the cold WBTs at the optimized EGR flow rates for the Side Injection Nozzles indicated that the average temperature at the fan was approximately 333 K. In order to match mass flow rate of the EGR gas with the replicate EGR gas a temperature correction was applied and flow rates of 44.7 to 62.6 SLPM were used (where SLPM is according to Alicat Mass Flow controller specs, 298 K and 14.7 psi). In total, three cold start WBT replicates were completed using the EGR replicate gas.

5.2.2 Chemicals Effects of CO_2/O_2 Recirculation

In order to replicate/isolate the chemical effect of O_2, pure molecular O_2 was injected into the stove using the Side Injection Nozzle configuration. Two important considerations must be made in order to accurately replicate the chemical effect of O_2 seen in the optimized EGR stove test. One, the mass flow rate of pure injected O_2 must be equivalent to the mass flow rate of O_2 injected in the optimized EGR stove test. Considering that the EGR gas was comprised of approximately 15% O_2, a flow rate equivalent to 15% of the temperature corrected optimized flow rates must be used. This leads to flow rates for pure O_2 injection of 6.7 and 9.4 SLPM for the start-up and steady-state firepower phases, respectively. Second, the velocity of the injected O_2 must be similar to the velocity of the injected EGR gas in order to mimic the injection

depth of the gas into the combustion chamber. In order to match the velocities between tests, the diameter of the holes through which gas escapes in the Side Injection Nozzles was modified such that the new hole area was equal to 15% of the original area. Three cold start WBT replicates were completed in which pure O_2 was injected into the stove.

In order to replicate/isolate the chemical effect of CO_2, pure CO_2 was injected into the stove. Because CO_2 comprises approximately 5% of the EGR gas, a flow rate equivalent to 5% of the temperature corrected optimized flow rates must be used. This leads to flow rates for pure CO_2 injection of 2.2 to 3.1 SLPM for the start-up and steady-state firepower phases, respectively. Because these flow rates are significantly lower than the total draft through the stove, matching the injection depth with the Side Injection Nozzles would be very difficult. To accommodate this issue the Diffusion Nozzle setup was used. This ensured that the natural draft of the stove carried the CO_2 in to the combustion chamber in a central location of the flame. Three WBT replicates were completed.

Because the CO_2 flow rates that mimic EGR gas comprised of 5% CO_2 were extremely low, additional tests were run with higher CO_2 flow rates to make any chemical/physical effects more evident. The same procedure as used in the pure O_2 injection tests was followed, instead replicating the chemical effect of CO_2 in EGR gas that is comprised of 15% CO_2. Three WBT replicates were completed.

5.2.3 Mixing, Dilution and Temperature Reduction due to Recirculated Nitrogen

To complete this study, Argon was injected at the optimized EGR flow rates through the side injection nozzles. In total, three cold start WBTs were completed

Initially, it was attempted to run these tests using pure Nitrogen, replicating exactly the mixing, dilution and temperature reduction effects of recirculated Nitrogen. However the heat capacity of the nitrogen made it impossible to maintain flame. Thus Argon was selected for

these tests because it has half the heat capacity of Nitrogen. Argon's low heat capacity allows for a better understanding of the effects of cooling of the flame, without cooling the flame so much that combustion cannot be maintained.

Additionally, its inert nature allows for the isolation of mixing, dilution and cooling effects by taking any intrinsic chemical effects out of the equation.

5.2.4 Firepower

In order to isolate the effect of increased firepower observed with the EGR tests in Section 4.4.3, the expected PM emissions at the measured firepower in the EGR stove are compared with the baseline M5000 emissions using the same fuel feeding approach.

Additionally, all tests completed in this section were compared to the expected baseline emissions based on measured firepower, using the relationship between Firepower and PM emissions in the baseline stove derived in section 3. This allowed for a more accurate isolation of the effects of each tested mechanisms.

5.3 Results/Discussion

All tests were completed using the Side Injection Nozzle configuration and referenced the optimized flow rates of 50 to 70 SLPM determined in Section 4. Thus, the magnitude of each mechanism's effect on PM emissions should be compared to the PM emissions reduction observed in the EGR tests with the Side Injection Nozzles, seen in Table 11. As a reminder to the reader, the average cold start water boil test PM emissions achieved with this optimized EGR configuration was 150 mg/MJd.

5.3.1 Increased Particle Residence Time

In the EGR stove a portion of the particulate matter is recirculated through the flame. This will results in a decrease of the net $PM_{2.5}$ mass emitted, assuming that oxidation is the net dominating mechanism along the particle's path. As indicated in section 2.4, formation and oxidation rates begin to compete at temperatures of approximately 800 ^{o}C. Fortunately, temperature profiles measured in a rocket elbow stove exceed 800 ^{o}C in a large portion of the combustion chamber [12]. This implies that oxidation may exceed formation rates and that particle recirculation through the flame may play a large role in reducing $PM_{2.5}$ emissions.

The effect of recirculating the $PM_{2.5}$ and consequently increasing its oxidation time was isolated by completing a set of cold start WBTs that used particle-free EGR replicate gas, composed of 80% N_2, 15% O_2 and 5% CO_2. The results of these tests can be seen in Table 13.

Table 13. EGR Replicate Gas Test Results

Test Description	EGR Replicate Gas Injection	
Number of Tests Completed	3	
	Mean	80% CI
Time to Boil (min)	24.1	22.4 – 25.9
Temperature Corrected Time to Boil (min)	24.0	22.4 – 25.6
Fuel Use to Boil (g)	308	301 – 316
FP kW	3.4	3.2 – 3.6
CS Thermal Efficiency (%)	33	32 – 34
PM (mg)	294	205 – 384
PM per Energy Delivered (mg/MJd)	180	130 - 240

In section 3, it was determined that firepower plays a large role in PM emissions, and a model for the baseline M5000 $PM_{2.5}$ emissions was proposed. In order to better isolate the effect of particle recirculation, the tests detailed in Table 13 are compared to the expected

baseline M5000 emissions based off of the measured firepower for these tests. This allows for the comparison of emissions produced from the tests in Table 13 to baseline emissions at the same firepower, taking firepower out of the equation and allowing for more accurate experimental isolation of the mechanism of interest. This comparison is detailed in Table 14.

Table 14. EGR Replicate Test Results Compared to Firepower Corrected Baseline

Average $PM_{2.5}$ (mg/MJ_d) for EGR Replicate Gas Tests	180
Average Measured FP (kW)	3.4
Predicted Baseline $PM_{2.5}$ (mg/MJ_d) at Measured FP	440

It can be seen in Table 14 that a reduction from 440 (mg/MJ_d) to 180 (mg/MJ_d) was achieved using particle-free EGR replicate gas. This indicates that a large portion of the $PM_{2.5}$ emissions reduction observed in the EGR stove was not caused by particle recirculation, but was instead caused by the chemical and physical effects of the gaseous component of the recirculated exhaust products. However, the resulting emissions for the particle free EGR replicate gas tests are slightly higher than the optimized EGR stove emissions of 150 (mg/MJ_d). This may imply that particle recirculation accounted for the small reduction in emissions from 180 (mg/MJ_d) to 150 (mg/MJ_d).

5.3.2 Chemical Effects of CO2/O2 Recirculation

Previous measurements of the recirculated gas indicated that it was composed of approximately 15% O_2, 5% CO_2, and 80% N_2 on average during the optimized EGR stove cold start WBTs. Other gaseous constituents may include carbon monoxide and argon but their concentrations were sufficiently low to deem their effects negligible. Given that N_2 acts nearly as a practically inert gas due to the relatively low combustion temperatures experienced during biomass combustion in rocket elbow stoves, it can be assumed that the major chemical effects may result from O_2 and CO_2 recirculation.

The results of the tests to isolate the chemical effects of O_2 and CO_2 can be seen in Table 15. Note, that the "pure O_2 injection at 15% of the optimized flow rate" and "pure CO_2 injection at 5% of the optimized flow" tests directly replicate their respective chemical effects in EGR gas that is composed of 15% O_2 and 5% CO_2. The "pure CO_2 injection at 15% of the optimized flow" tests were completed in order to make any potential chemical effects of CO_2 more evident. Given that the recirculated gas must always be 80% N2, a 15% CO_2 composition would indicate that the stove is operating near with near stoichiometric levels of total draft. Because rocket elbow stoves typically operate with significantly fuel lean concentrations, then replicating a 15% CO_2 composition can be assumed to be an estimate for the absolute maximum potential chemical effect of CO_2.

Table 15. Effects of CO_2 and O_2 Test Results

Test Description	Pure O_2 Injection 15% of Optimized Flow		Pure CO_2 Injection, 5% of Optimized Flow		Pure CO_2 Injection, 15% of Optimized Flow	
Number of Tests Completed	3		3		3	
	Mean	80% CI	Mean	80% CI	Mean	80% CI
Time to Boil (min)	25.2	24.2 – 26.2	29.3	27.7 - 30.9	26.7	25.9 – 27.6
Temperature Corrected Time to Boil (min)	25.0	24.0 – 26.1	29.2	27.5 – 30.8	26.7	25.6 - 27.7
Fuel Use to Boil (g)	280	271 – 288	287	285 – 290	297	289 – 304
FP kW	3.0	2.8 – 3.2	2.5	2.3 – 2.7	2.9	2.9 – 3.0
CS Thermal Efficiency (%)	36	35 – 37	37	35 – 39	36	35 – 36
PM (mg)	167	147 – 186.4	523	467 - 578	540	387 – 692
PM per Energy Delivered (mg/MJd)	100	90 – 110	320	290 – 360	320	240 - 410

The test results detailed Table 15 are compared in Table 16 to the expected baseline M5000 emissions based off of the measured firepower for these tests. This allows for a more accurate isolation of the chemical effects of interest, by taking firepower variations out of the equation.

Table 16. Effects of CO_2 and O_2 Test Results Compared to Firepower Corrected Baseline

Test Description	Pure O2 Injection 15% of Optimized Flow	Pure CO2 Injection, 5% of Optimized Flow	Pure CO2 Injection, 15% of Optimized Flow
Average $PM_{2.5}$ (mg/MJ_d)	100	320	320
Average FP (kw)	3.0	2.5	2.9
Average FP Corrected Baseline $PM_{2.5}$ (mg/MJ_d)	260	300	320
Percent Reduction in $PM_{2.5}$ from Predicted Baseline	61%	- 8%	- 2%

It can be seen in Table 16 that pure O_2 injection leads to a dramatic reduction in mass of PM emitted. The visually observed mixing effect throughout these tests was negligible, and it can be assumed that the O_2 concentration near the fuel was unaffected. However, it was visually observed that the O_2 was injected sufficiently into the flame near the top of the combustion chamber, such that the streams of injected O_2 on either side of the combustion chamber converged as they entered the chimney of the M5000. Thus, it can be concluded that a significant reduction in $PM_{2.5}$ mass occurred and was due primarily to a chemical effect caused by elevating the concentrations of O_2 within the region of the flame above the fuel.

The isolated chemical effects of CO_2 do not appear to cause any significant effect on the mass of $PM_{2.5}$ emitted. Literature has indicated that the effect of elevated CO_2 concentration only causes significant reductions in soot precursors at high temperatures above approximately 1500K [13]. A study of the temperature profile within a rocket elbow stove indicated that the peak combustion temperature is around 1500K, with most of the combustion chamber below this value [14]. This corresponds with the measured data, indicating that the chemical effect of CO_2 across the range of potential concentrations has an insignificant effect on PM emissions.

5.3.3 Mixing, Dilution and Temperature Reduction

In order to better understand the various effects of recirculating nitrogen through the Side Injection Nozzles, Argon was injected at the optimized EGR stove flow rates. Three cold start WBT's were completed using Argon injection at the optimized flow rates, the results of which can be seen below in Table 17.

Table 17. Effects of Mixing, Dilution and Temperature Reduction Test Results

Test Description	Argon Injection at Optimized Flows	
Number of Tests Completed	3	
	Mean	80% CI
Time to Boil (min)	26.1	24.3 – 27.9
Temperature Corrected Time to Boil (min)	26.3	24.4 – 28.2
Fuel Use to Boil (g)	317	315 – 319
FP kW	3.1	2.9 – 3.3
CS Thermal Efficiency (%)	34	33 – 34
PM (mg)	618	504 – 733
PM per Energy Delivered (mg/MJd)	380	310 – 450

As described in previous sections, the tests results detailed Table 17 are compared in Table 18 to the expected baseline M5000 emissions based off of the measured firepower for these tests. This allows for a more accurate isolation of the mechanisms of interest by taking firepower variations out of the equation.

Table 18. Effects of Mixing, Dilution and Temperature Reduction Test Results Compared to Firepower Corrected Baseline

Test Description	Argon Injection
Average $PM_{2.5}$ (mg/MJ_d)	380
Average FP (kw)	3.1
Average Expected Baseline $PM_{2.5}$ (mg/MJ_d)	340
Percent Reduction in $PM_{2.5}$ from Predicted Baseline	-10%

It can be seen in Table 18 that the effect of injecting Argon caused a minor increase in $PM_{2.5}$ emissions. This minor increase in emissions is the net result of a combination of enhanced mixing, reactive constituent dilution and temperature reduction.

In order to better understand the individual effects of these three mechanisms, we will first consider mixing. For this test set, the optimized EGR stove mass flow rates were matched with Argon. Every recirculated exhaust gas molecule was replaced with an Argon molecule that injected at the same velocity. Consider that mixing is a function of the particle momentum, and consider that Argon's molecular weight is 40 (kg/kmole) whereas the recirculated exhaust gas molecular weight is approximately 29 (kg/kmole). Because Argon's molecular weight is larger, its momentum and mixing effect will be approximately 38% larger.

The effect of enhanced mixing in the combustion processes of solid biomass fuels has been documented to reduce emissions of carbonaceous particles. Emissions of soot and soot precursors are compounded by poor mixing where pockets of unburned vapors and particles may exit the combustion zone [15]. Thus, it is assumed that the isolated effect of the mixing caused by the Argon reduces $PM_{2.5}$ emissions.

However, the total effect of Argon injection actually led to an increase in $PM_{2.5}$ emissions. Thus, Argon's combined effects of dilution and temperature reduction actually caused an increase in $PM_{2.5}$ emissions. In order to better understand the effect of cooling on the flame, a comparison is made between the cooling capacity of the recirculated nitrogen in the optimized

EGR stove, and the cooling capacity of the injected Argon. The heat capacity of Argon is 0.52 (kJ/(kg-K)) and the heat capacity of N_2 is 1.04 (kJ/(kg-K)). Additionally, the calculated mass flow rate during the steady state phase is 114 g/min for Argon and 83 g/min for the recirculated N_2. Given that the initial injection temperatures for both gases remained near ambient, it can be concluded that the cooling effect (which is approximated by multiplying the mass flow rate and the heat capacity for both gases) of the recirculated N_2 was approximately 45% larger than that of the Argon. This indicates that the recirculated N_2 in the EGR stove will have a larger effect on emissions. Ultimately, literature indicates that the effect of cooling the flame in small biomass combustion applications will increase the mass emissions of particles [15]. This may be explained by an expansion of cooler regions less than approximately 800 ^{o}C, where particle growth tends to be greater than particle oxidation [8].

This isolated effect of dilution of the reactive components in solid biomass combustion is not easy to discern from this test data. Additionally, this effect is not well documented in literature. Consequently, the combined effects of dilution and temperature reduction are grouped together as one emissions mechanism that us observed to cause an increase in $PM_{2.5}$ emissions.

5.3.4 Firepower

In the tests using EGR at the optimized flow rates through the side injection nozzles, it was observed that the firepower unintentionally increased. This is due to the forcing of oxidizer onto and near the surfaces of the sticks. In order to isolate the effect of the increased firepower observed with the optimized EGR tests the expected PM emissions at the measured firepower in the EGR stove are compared with the baseline M5000 emissions using the same fuel feeding approach.

Table 19. Effect of Firepower Increase from Application of EGR

Test Description	EGR at optimized flow rates
Average FP for Optimized EGR tests(kW)	2.9
Average Predicted Baseline $PM_{2.5}$ (mg/MJ_d) from Optimized EGR tests	310
Average Baseline $PM_{2.5}$ (mg/MJ_d) using 3 stick feeding approach	280
Percent Reduction in $PM_{2.5}$ from Predicted Baseline	-12%

The results seen in Table 19 indicate that the isolated effect of increased firepower resulting from the application of EGR led to a slight increase in PM emissions.

5.4 Understanding EGR Emissions Reductions Mechanisms General Conclusions

The experimental optimization of the EGR stove led to a reduction in $PM_{2.5}$ mass emissions. The optimized configuration reduced emissions from a baseline value of 280 mg/MJ_d, to an optimized value of 150 mg/MJ_d. The optimized stove utilized side injection nozzles that injected recirculated exhaust gas into the oxidation zone of the flame, and forced mixing and an increase in fuel consumption rate. In order to better understand the driving forces behind net emissions reduction, potential mechanisms that can affect $PM_{2.5}$ mass were identified and their effects were isolated experimentally.

It was determined that the mechanisms for reducing $PM_{2.5}$ mass emissions include the chemical effect due to injecting the optimized O_2 concentration within into the flame above the fuel, increased residence time of particles in the flame via recirculation and enhanced mixing. Out of the mechanisms that reduce $PM_{2.5}$ emissions, it was shown that the chemical effect of injecting the optimized O_2 concentration is the most prominent. The isolated effect of CO_2 recirculation was determined to have no significant effect on $PM_{2.5}$ emissions. Additionally, the combined effects of temperature reduction and dilution due to recirculated Nitrogen, and the

isolated effect of the increased the fuel consumption rate due to the application of EGR likely lead to increases in $PM_{2.5}$ emissions. However, when these mechanisms effects are combined, a net reduction in $PM_{2.5}$ mass emitted is observed.

6 Comparison of EGR with Air Injection

It was found that one of the primary mechanisms for emissions reduction in the EGR stove was the chemical effect of O2 when injected into the oxidation region of the flame. These results indicate that a stove that utilizes air injection in a similar fashion as the EGR stove side injection nozzles configuration may lead to similar or greater emissions reductions. A study was conducted to confirm this hypothesis, and to understand the relative impacts between the two fundamentally different forced draft systems.

6.1 Testing Methodology

The M5000 was used for these tests. For the forced draft air injection system, compressed air regulated by an Alicat Mass Flow Controller was routed through the side injection nozzles. The side injection nozzles were the same as those used in section 4, with 12 holes at 4.9 millimeter diameter that inject air perpendicularly to the natural draft of the stove at the top of the combustion chamber.

In order to make a fair comparison between EGR and air injection, the minimized PM emissions for each forced draft system were determined for the side injection nozzles configuration. The minimized emissions for this configuration using EGR were previously determined in Section 4. In order to determine the minimized emissions using air injection, the same procedure, as outlined in section 4.4.3 was followed. Once the minimized emissions for each forced draft system were determined, a comparison was made.

6.2 Results/Discussion

The results of air flow rate optimization tests can be seen below in Figure 31.

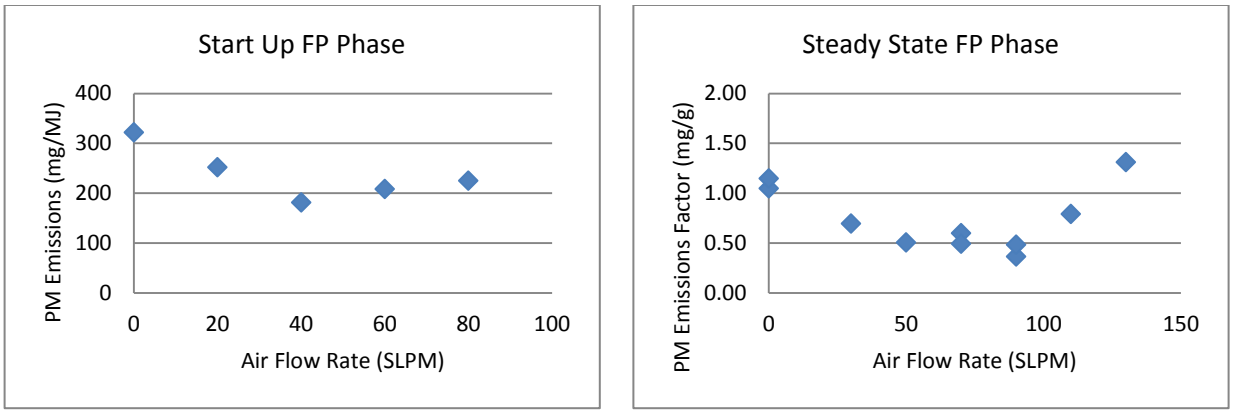

Figure 31. Air Injection Flow Rate Optimization for Side Injection Nozzles

The optimized flow rates using air injection were determined to be 40 and 80 SLPM for the start up and steady state phases, compared to the optimized EGR flow rates of 50 and 70 SLPM. The results of the three cold start WBTs using the optimized air flow rates, and the previously defined results of the optimized EGR flow rates tests are seen below in Table 20.

Table 20. Air and EGR Comparison

Forced Draft	Air		EGR
Number of Tests Completed	3		2
	Mean	80% CI	Mean
Time to Boil (min)	21.2	19.5 – 23.0	28.9
Temperature Corrected Time to Boil (min)	21.2	19.3 – 23.1	32.1
Fuel Use to Boil (g)	307	303 – 311	317
FP kW	3.8	3.6 – 3.9	2.9
CS Thermal Efficiency (%)	35	34 – 35	32
PM (mg)	138	113 – 162	248
PM per Energy Delivered (mg/MJd)	83	71 – 95	150
Percent Reduction from Baseline (%)	70%	-	44%

The results in Table 20 indicate that the air injection stove performed better than the EGR stove, with a total overall emissions reduction of 70% compared to 44%. As was discovered in the “Understanding EGR Stove Emissions Reduction” section, elevation of the O2 concentration

in the oxidation region of the flame was a major factor in contributing to the emissions reduction. An air injection stove can force higher concentrations of O2 without diluting or cooling the flame as much as an EGR stove, where the recirculated exhaust gas is partly comprised of CO2, thus increasing the total chemical effect of O2.

These results proved that air injection is the higher performing and more practical solution for a forced draft system in a rocket elbow cookstove. Consequently, the remainder of this study focuses on further optimization of air injection methods, and not EGR.

It should be noted that there is a possibility that different nozzle configurations may perform better for EGR than for air injection, or vice versa. However, the side injection nozzles were selected for the comparison study because it was expected that the final design of the forced draft stove would likely use a similar configuration.

7 Optimization of Air Injection Nozzle Diameter for Side Injection Nozzles

After the discovering that a forced draft air system will outperform an EGR system for the case of small rocket elbow stoves, it was decided that the study would proceed with further nozzle optimization using only air injection. In section 7 the effect of changing the hole diameter of the side injection nozzles while using a fixed injection location and a fixed number of holes is explored.

7.1 Testing Methodology

The M5000 was used for these tests. For the forced draft air injection system, compressed air regulated by an Alicat Flow Controller was routed through the side injection nozzles. The side injection nozzles were located at the top of the combustion chamber, in a parallel orientation with 6 holes per nozzle.

Four different diameters were tested, including 2.3, 3.2, 4.9 and 5.7 mm. For each diameter, the flow rate optimization as described in section 4.3.3 was completed. Three cold start WBTs were then completed for each diameter at the optimized flow rates.

7.2 Results/Discussion

7.2.1 Nozzle Diameter and Optimized Flow Rate

The major results of the flow rate optimization for each diameter can be seen in Table 21. Detailed results of flow rate sweep testing can be found in Appendix A.

Table 21. Nozzle Diameter Optimization Results for Side Injection Nozzles

Nozzle Diameter (mm)	5.7		4.9		3.2		2.3	
Optimized Start-up Flow (SLPM)	20		40		40		20	
Optimized Steady-state Flow (SLPM)	80		80		80		60	
Number of Cold Start Tests	3		3		3		3	
	Mean	80% CI	Mean	80% CI	Mean	80% CI	Mean	80% CI
Time to Boil (min)	25.7	23.8 - 27.7	21.2	19.5 – 23.0	25.5	22.4 - 28.5	22.3	20.6 - 24.0
Temperature Corrected Time to Boil (min)	25.7	23.8 - 27.7	21.2	19.3 - 23.1	25.5	22.6 - 28.4	22.3	20.8 - 23.8
Fuel Use to Boil (g)	301	293 - 308	307	303 - 311	313	305 - 321	301	297 - 305
FP kW	3.1	2.8 - 3.3	3.8	3.6 - 3.9	3.2	2.9 - 3.5	3.6	3.4 - 3.9
CS Thermal Efficiency (%)	34	34 - 35	35	34 - 35	33	32 - 33	33	33 - 34
PM (mg)	144	125 - 162	138	113 - 162	131	103 - 160	141	97 - 184
Optimized $PM_{2.5}$ Emissions (mg/MJ)	89	78 - 100	83	71 - 95	82	64 - 99	89	60 - 110
% Reduction from Baseline $PM_{2.5}$ Emissions	68%	N/A	70%	N/A	70%	N/A	68%	N/A

The reduction in $PM_{2.5}$ emissions from the baseline M5000 $PM_{2.5}$ emissions data are presented for comparison. It can be seen that significant $PM_{2.5}$ emission reductions of

approximately 70% from baseline were achieved for each of the nozzle diameters tested (p = 0.03, 0.02, 0.02 and 0.02 for diameters of 5.7, 4.9, 3.2 and 2.3 mm, respectively).

It can be seen that the optimized flow rates are very different between the start-up phase and steady state phase. This indicates that, as hypothesized in section 3, the optimized flow rate is a strong function of firepower.

It should also be noted that the optimized steady state flow rates tend to decrease slightly as the diameter decreases. This can be explained by the observed elevated tendency of smoke to spurt out the front of the combustion chamber at higher forced draft velocities. This effect limits the flow rates through small diameter and higher velocity nozzles.

7.2.2 Nozzle Diameter and PM Emissions

Figure 32 presents the optimized $PM_{2.5}$ emissions as a function of the nozzle diameter. The error bars represent the 80% confidence interval for each set of tests.

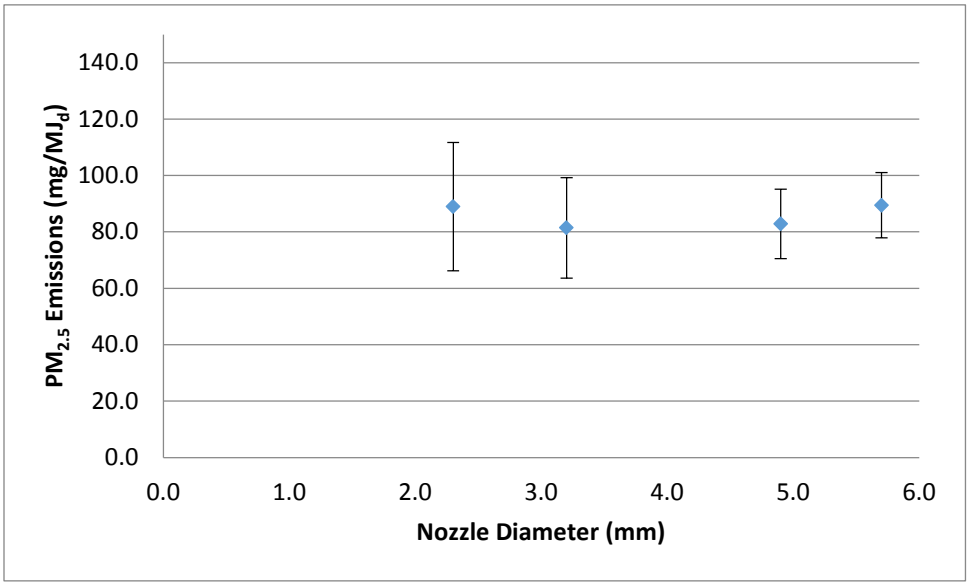

Figure 32. Optimized $PM_{2.5}$ Emissions as a function of Nozzle Diameter for Side Injection Nozzles

It can be seen that the optimized $PM_{2.5}$ emissions are similar across the entire range of diameters tested, indicating that if the optimized flow rates are used, the various diameters will produce similar emissions reductions.

Figure 33, seen below, display the velocity of the injected air at the steady state flow rates for each of the diameters. Again, the error bars also represent the 80% confidence interval for each set of tests. The data points from left to right represent the 5.7, 4.9, 3.2 and 2.3 mm diameters.

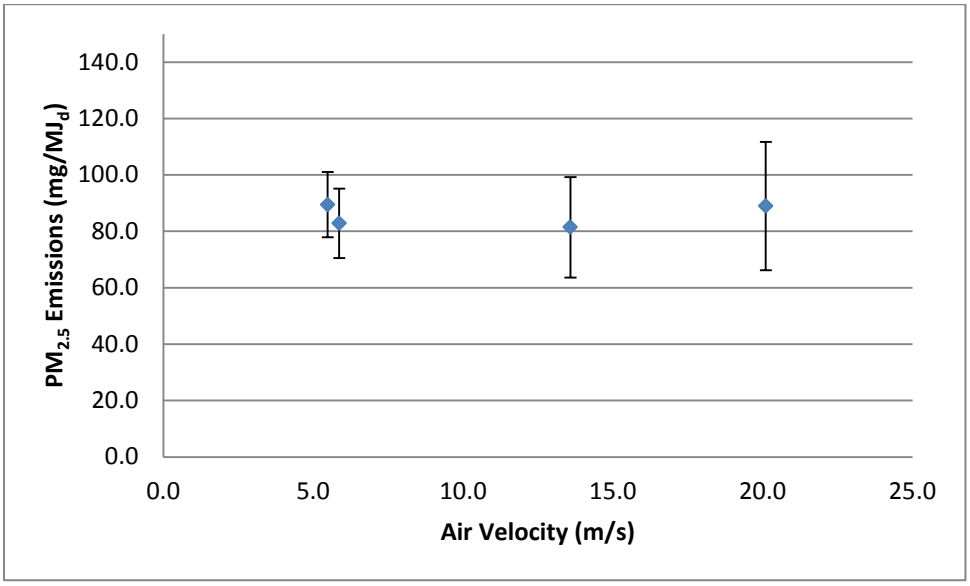

Figure 33. Steady State Flow Velocities and Optimized Emissions for Various Diameters

In Figure 33, it can be seen that velocity of the injected air increases significantly as the side injection nozzle hole diameter decreases, but the optimized PM emissions remain relatively constant. This implies that for the range of diameters tested and if the optimized flow rates are used, then the velocity is not important. In other words, it may imply a sufficient level of mixing from a velocity of 5 to 20 meters/second.

Another conclusion that may be drawn from Figure 33 is that the dispersion of the optimized emissions tends to increase as velocity increases. This can be explained, as previously

mentioned, by the observed elevated tendency of smoke to spurt out the front of the combustion chamber at higher forced draft velocities.

7.2.3 Local Peak Emissions Behavior

During the flow rate sweep tests an interesting localized peak emissions behavior was observed at a few instances. Examples of this local peak behavior are seen below at 30 SLPM in Figure 34 and 40 SLPM in Figure 35, where Figure 34 displays the results of the forced draft flow rate sweep for the for the start-up phase for the 3.2 mm diameter nozzles and where Figure 35 displays the results of the forced draft flow rate sweep for the steady-state phase for the 5.7 mm diameter nozzles.

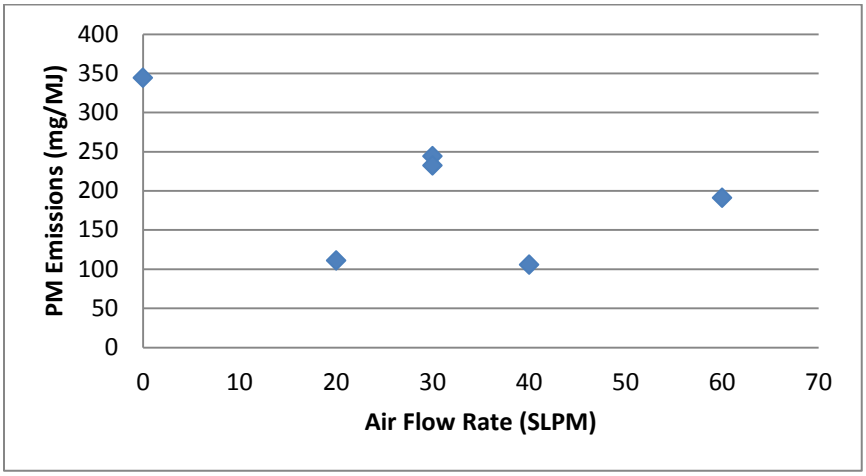

Figure 34. Local Peak Emissions Example 1

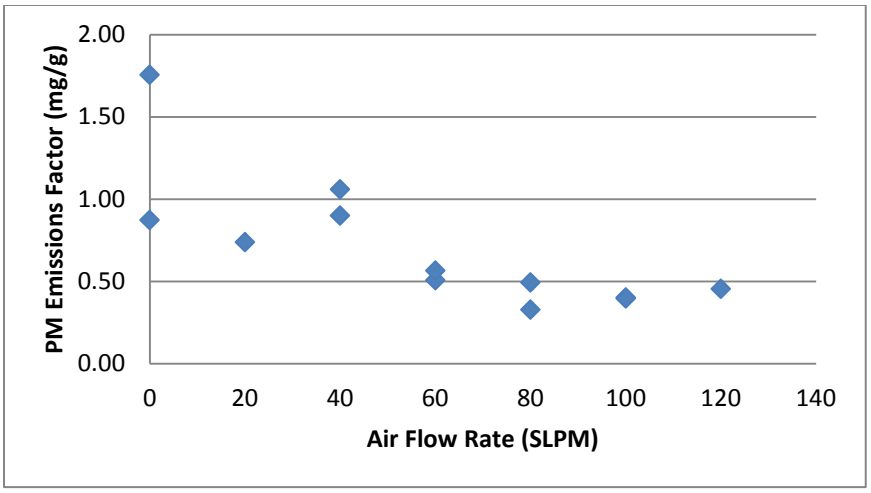

Figure 35. Local Peak Emissions Example 2

Visual observations of the flame and fluid flow characteristics help to provide justification for these local peaks in emissions. The observed flow patterns are depicted in Figure 36.

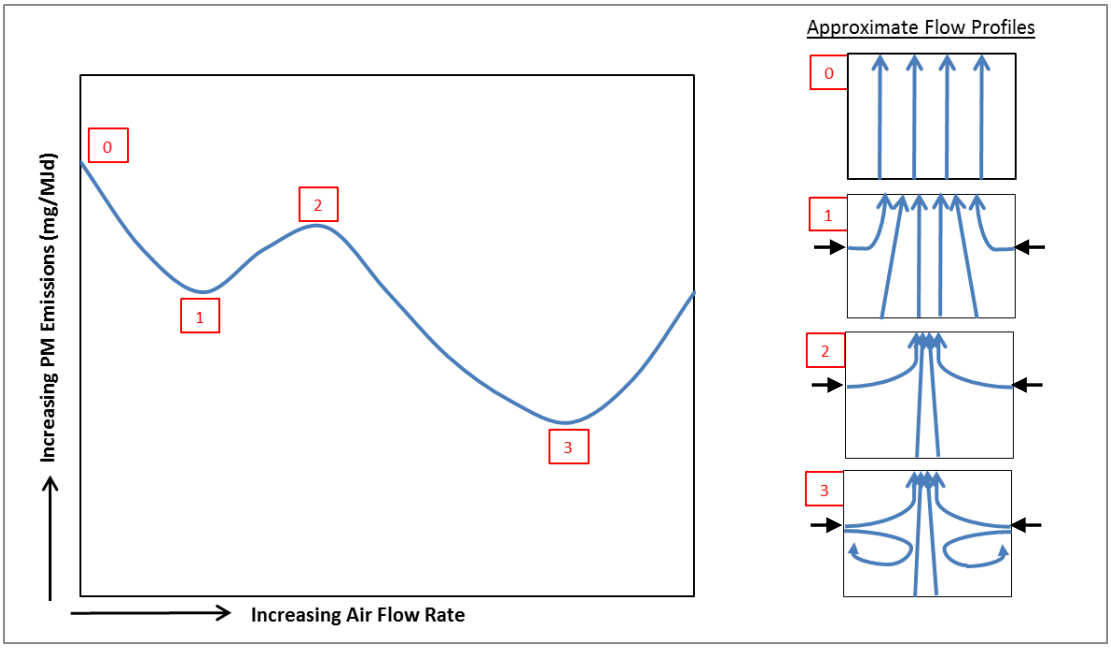

Figure 36. Flow Profiles in Combustion Chamber at Varied Air Injection Flows Rates and Effect on Emissions

The flow profiles pictured on the right side are rough depictions of the flow through the combustion chamber, with side injection nozzles supplementing the flow for profiles 1 through 3 at the black arrows.

Point 0 represents an undisturbed natural draft through the combustion chamber, with no forced draft. At point 1, which would be at approximately 20 SLPM in Figure 35, the oxidation region of the flame is supplemented therefore decreasing the PM emissions, but no mixing is occurring below the height of the side injection nozzles. At point 2, which would be at approximately 40 SLPM in Figure 35, the forced draft is strong and concentrated enough to quench the oxidation region of the flame at the height of the nozzles, but not strong enough to induce mixing below the nozzles. The quenching of the oxidation region of the flame causes a local increase in PM emissions. At point 3, which would correspond to flow rates of 60 SLPM and greater in Figure 35, the forced draft is strong enough to slightly overcome the natural draft of the stove and induces mixing throughout the combustion chamber. This more evenly distributes the forced draft, allowing for higher forced draft flow rates without the consequence of quenching the flame, and ultimately causing significant reductions in PM emissions.

This effect was not observed in all of the flow rate sweeps. It may be postulated that this effect would have been observed in all of the flow rate sweeps if a finer flow rate sweep resolution had been used.

8 Optimization of Air Injection Location

To further the optimization the air injection method the injection location was evaluated. In section 8, various injection locations are explored in the G3300.

8.1 Testing Methodology

8.1.1 Comparison of G3300 and M5000 PM Emissions Performance

Project funding necessitated the use of the G3300 for this section and any further testing in this document. The G3300 is similar in design to the M5000, with a few slight differences. The G3300 is insulated around the combustion chamber, whereas the M5000 uses an aluminum radiation shield. The G3300 has a slightly larger combustion chamber with a wider opening than the M5000. Lastly, the G3300 ceramic base is smaller than the M5000 ceramic base. Otherwise, both stoves have similar chimney dimensions. It was found in section 3 that these differences cause a difference in baseline $PM_{2.5}$ emissions between the two stoves. However, an additional comparison was made between the performances of the stoves when a forced draft is applied. This second comparison was completed to ensure that the forced draft knowledge gained from previous work on the M5000 could be extended to work on the G3300.

A comparison between the minimized $PM_{2.5}$ emissions and optimized flow rates for each stove was completed using the side injection nozzles with a diameter of 2.3 mm. The minimized $PM_{2.5}$ emissions and optimized flow rates for each stove were determined using same procedure outlined in section 4.4.3.

8.1.2 Injection Location

A comparison between the minimized $PM_{2.5}$ emissions and optimized flow rates for 4 injection locations were tested, including the top of the combustion chamber and the bottom, middle and top of the chimney section. Figure 37 presents a cross sectional view of the G3300 rocket elbow style design, with the general injection locations labeled. The distance from the top of the ceramic base in the centimeters are also labeled.

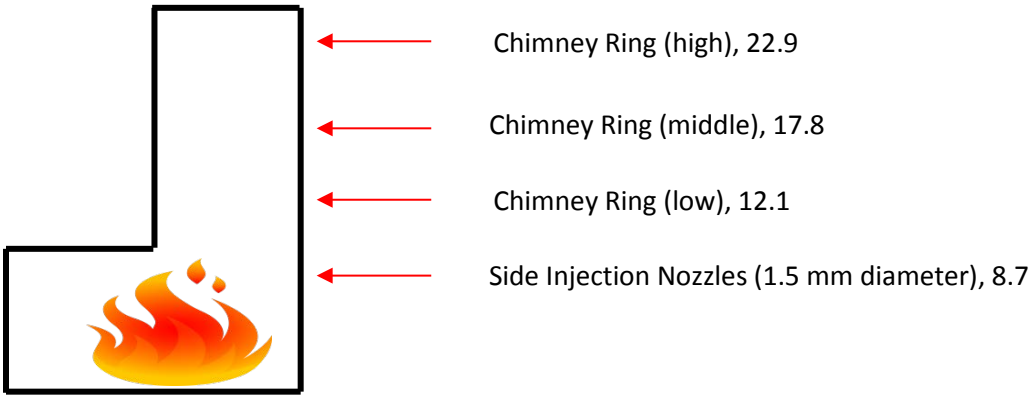

Figure 37. Injection Locations Tested in G3300

In order to test the top of the combustion chamber injection location, the side injection nozzles were used. In order to test injection locations within the chimney section, a "chimney ring" nozzle was fabricated. Figure 38 displays the chimney ring nozzle used in the lowest portion of the chimney. It can be seen that the chimney ring style nozzles inject air horizontally and towards the vertical axis of the chimney.

Figure 38. Chimney Ring Nozzle

For all of the nozzles in this section, 12 holes were used with 1.5 mm diameters. A diameter of 1.5 mm was selected because preliminary studies indicated that the chimney ring style nozzles with larger diameters would quench the flame at low flow rates, causing significant smoke and flames to be emitted out of the front of the combustion chamber. Using a small diameter prevented quenching of the flame and allowed for higher forced draft flow rates to be used. Further justification for the selection of the 1.5 mm diameter for the injection location study is provided in section 9. Lastly, 12 holes were used ensure adequate distribution of the forced draft across the entire flame and to maintain consistency with previous work.

8.2 Results/Discussion

8.2.1 Comparison of G3300 and M5000 PM Emissions Performance

Table 22 presents the major results of the comparison of the optimized $PM_{2.5}$ emissions between the G3300 and M5000 when using the side injection nozzles with a 2.3 mm diameter. The mean values represent the average of 3 tests.

Table 22. Comparison of M5000 and G3300 Emissions Performance and Optimized Flow Rates with Similar Configuration

Stove	M5000		G3300	
Optimized Start-up Phase Flow Rate (SLPM)	20		30	
Optimized Steady-state Phase Flow Rate (SLPM)	60		60	
	Mean	80% CI	Mean	80% CI
Time to Boil (min)	22.3	20.6 – 24.0	22.2	21.5 – 22.9
Temperature Corrected Time to Boil (min)	22.3	20.8 – 23.8	22.1	21.3 – 22.9
Fuel Use to Boil (g)	301	296 – 305	325	306 – 345
FP kW	3.6	3.4 – 3.9	3.9	3.7 – 4.2
CS Thermal Efficiency (%)	33	33 – 34	31	30 – 33
PM (mg)	141	97 - 184	135	84 - 186
PM per Energy Delivered (mg/MJd)	87	60 - 110	82	53 - 110
Percent Reduction from Baseline PM (%)	68%	N/A	78%	N/A

It can be seen that the optimized flow rates for both stoves are similar. This indicates that the slight geometric differences between the two combustion chambers do not lead to significant differences or limitations for the optimized forced draft flow rates. This also implies that the optimized forced draft flow rates will similar between both stoves for other nozzle configurations.

Additionally, it can be seen that the $PM_{2.5}$ emissions for both stoves are not significantly different ($p=0.82$). This indicates that the optimized $PM_{2.5}$ emissions performance measured in previous work with the M5000 may be comparable to optimized $PM_{2.5}$ emissions performance with the G3300, and that the differences between the two stoves performance is not so apparent when the optimized flow rate is applied.

8.2.2 Injection Location

Table 23 presents the major results of the injection location study. More detailed results of flow rate sweep testing can be found in Appendix A.

Table 23. Injection Location Optimization Results

Injection Location (cm)	Top of Chamber (8.7)		Bottom of Chimney (12.1)		Middle of Chimney (17.8)		Top of Chimney (22.9)	
Start-up Flow (SLPM)	20		20		20		10	
Steady-state Flow (SLPM)	40		40		40		10	
Number of Tests	3		3		3		3	
	Mean	80% CI	Mean	80% CI	Mean	80% CI	Mean	80% CI
Time to Boil (min)	21.1	20.5 - 21.7	15.0	13.5 - 16.6	19.3	16.5 - 22.1	21.8	20.5 - 23.1
Temperature Corrected Time to Boil (min)	21.2	20.3 - 22.0	15.0	13.4 - 16.7	19.3	16.6 - 22.1	21.8	20.5 - 23.0
Fuel Use to Boil (g)	304	287 - 322	320	293 - 346	331	310 - 351	276	271 – 281
FP kW	3.9	3.7 - 4.1	5.9	5.4 - 6.3	4.6	4.1 - 5.2	3.4	3.2 - 3.6
CS Thermal Efficiency (%)	33	31 – 34	31	28 – 34	30	28 – 33	36	35 – 37
PM (mg)	115	62 - 168	101	68 - 133	147	79 - 214	449	399 - 498
$PM_{2.5}$ Emissions (mg/MJ)	72	40 - 100	61	40 - 82	92	48 - 130	280	250 - 310
% Reduction from Baseline $PM_{2.5}$ Emissions	81%	N/A	84%	N/A	76%	N/A	26%	N/A

It can be seen that the optimized flow rates are similar across the bottom three injection locations. However, at the top injection location, the optimized flow rates drop down to 10 SLPM. Figure 39 is composed of images taken during the flow rate sweeps for the top injection location.

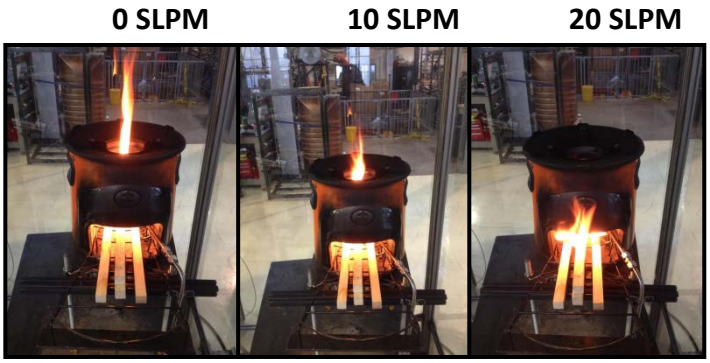

Figure 39. Air Flow Rate Effect at Top Injection Location

At a flow rate of 0 SLPM, the flame out of the top of the chimney is tall and wispy. At a flow rate of 10 SLPM the flame is shorter and more condensed. When a flow rate of 20 SLPM is used, the top of the flame is entirely quenched at the injection location. This causes a significant reduction in the draft through the stove, and leads to significant smoke and flame out of the front of the stove. Ultimately, this limits the optimized flow rate for the top of the chimney injection location to 10 SLPM, also limiting the $PM_{2.5}$ emissions reduction potential for this configuration. This phenomenon was much less significant for the lower injection locations because the flame is stronger and less susceptible to quenching.

Comparing the optimized PM emissions from the bottom three injection locations leads to the conclusion that bottom of the chimney is the optimized injection location. However, injection at the top of the combustion chamber also led to good performance. It may be hypothesized that these locations led to the largest reduction because they inject where the flame is the strongest and supplement the oxidation of particles without causing cooling or quenching of the flame.

Another important observation is the effect on time to boil and firepower for each injection location. It appears that the bottom of the chimney injection location leads to significant increase in firepower and a large decrease in time to boil, both features that may be quite valuable to the consumer.

Ultimately, injecting the forced draft at the bottom of the chimney is the optimal solution. It leads to significant emissions reductions from baseline ($p=0.001$) and is a relatively inconspicuous design when compared to the side injection nozzles, which intrude into the combustion chamber.

9 Optimization of Air Injection Nozzle Diameter for Chimney Ring Nozzle

In section 7, it was found that the diameter of the nozzle is not a strong determinant of the minimized PM emissions when the injection location is at the top of the combustion chamber, with the side injection nozzles. However, the minimized PM emissions may not be a weak function of diameter for other injection locations and nozzle configurations. Thus, in this section the effect diameter has on emissions for the chimney ring style nozzle located at the bottom of the chimney is explored.

9.1 Testing Methodology

The effect of nozzle diameter on emissions was tested for the chimney ring nozzle located at the bottom of the chimney in the G3300. Hole diameters of 1.5 and 3.0 millimeters were tested. For each diameter, the flow rate optimization as described in section 4.3.3 was completed. Three cold start WBTs were then completed for each diameter at the optimized flow rates. The resulting optimized emissions and flow rates were then compared.

9.2 Results/Discussion

The results of the diameter optimization for the chimney ring style nozzle are displayed below in Table 24.

Table 24. Diameter Optimization Results for Bottom of Chimney Injection Location

Nozzle Diameter (mm)	1.5		3.0	
Optimized Start-up Phase Flow Rate (SLPM)	20		20	
Optimized Steady-state Phase Flow Rate (SLPM)	40		20	
	Mean	80% CI	Mean	80% CI
Time to Boil (min)	15.0	13.5 - 16.6	23.3	22.7 - 23.9
Temperature Corrected Time to Boil (min)	15.0	13.4 - 16.7	23.5	22.9 - 24.1
Fuel Use to Boil (g)	320	293 - 346	283	280 – 285
FP kW	5.9	5.4 - 6.3	3.2	3.2 - 3.3
CS Thermal Efficiency (%)	31	28 – 34	35	35 – 36
PM (mg)	101	68 - 133	167	140 - 195
PM per Energy Delivered (mg/MJd)	61	40 - 82	100	87 – 120
Percent Reduction from PM Baseline	84%	N/A	72%	N/A

It can be seen that the 1.5 mm diameter nozzles had a larger optimized steady-state flow rate. This is because the 3.0 mm diameter nozzle caused quenching of the flame at flow rates greater than 20 SLPM, leading to the emissions of smoke and flames out of the front of the combustion chamber. It can also be seen that the optimized $PM_{2.5}$ emissions were significantly lower for the 1.5 mm diameter than for the 3.0 mm diameter ($p=0.04$). The quenching of the flame limited the forced draft flow rate which consequently limited the $PM_{2.5}$ emissions reduction.

This data indicates that for the chimney ring style nozzle, the optimized diameter is smaller than 3.0 mm.

10 Optimization of Air Injection Angle for Chimney Ring Nozzle

In Section 8 the optimized injection location was determined and in Section 9 the optimized diameter at the optimized location was determined. In section 10, the effect of altering the angle of injection for the optimized injection location and diameter is explored.

10.1 Testing Methodology

In order to understand the effect of injection angle the minimized emissions from two configurations were compared. The injection location used for these tests was at the bottom of the chimney, the optimal injection location found in section 8. The tested injection angles were either horizontal or 30^{o} above horizontal. Figure 40 displays the location of the two nozzles used in this study. Additionally, both nozzles used in this study had 12 holes with 1.5 mm diameters.

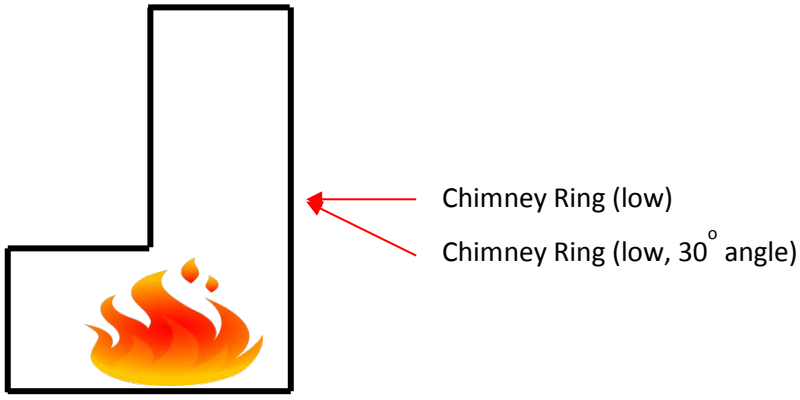

Figure 40. Injection Angles Tested at Bottom of Chimney

Figure 41 shows the chimney ring nozzle that injects at an angle of 30^{o} from horizontal.

Figure 41. Angled Chimney Ring Nozzle

10.2 Results/Discussion

Table 25 displays the results of the injection angle study. More detailed results of flow rate sweep testing can be found in Appendix A.

Table 25. Injection Angle Test Results

Injection Angle - Location	Horizontal – Bottom of Chimney		30^{o} upwards from Horizontal – Bottom of Chimney	
Optimized Start-up Phase Flow Rate (SLPM)	20		10	
Optimized Steady-state Phase Flow Rate (SLPM)	40		10	
	Mean	80% CI	Mean	80% CI
Time to Boil (min)	15.0	13.5 - 16.6	23.7	23.0 – 24.5
Temperature Corrected Time to Boil (min)	15.0	13.4 - 16.7	23.9	23.2 - 24.6
Fuel Use to Boil (g)	320	293 – 346	276	263 - 290
FP kW	5.9	5.4 - 6.3	3.1	3.1 - 3.2
CS Thermal Efficiency (%)	31	28 – 34	36	35 – 37
PM (mg)	101	68 - 133	199	186 - 211
PM per Energy Delivered (mg/MJd)	61	40 - 82	130	120 - 130
Percent Reduction from PM Baseline	84%	N/A	67%	N/A

It can be seen that the optimized flow rates for the 30^{o} injection angle is limited to 10 SLPM. Additionally, the emissions reduction achieved with the horizontal injection angle is greater than the emissions reduction achieved with a 30^{o} injection angle ($p=0.02$).

A lesser emissions reduction is achieved with the angled injection because the angle of the forced draft promotes a high total draft through stove. Increasing the total draft through the stove can cool the flame significantly, especially if there is not a high level of mixing. Cooling of the flame can increase the volume of regions of particle growth and decrease the regions of particle oxidation. Thus, it was concluded that a horizontal injection angle is the preferred solution.

11 Conclusions

Inefficient combustion of solid biomass for domestic cooking and heating presents a tremendous global problem to human and environmental health. Colorado State University's cookstove laboratory has challenged this problem by developing technology that reduces Particulate Matter emissions by over 80% from wood burning rocket elbow cookstoves, and by over 90% from traditional cookstoves.

11.1 PM Emissions from biomass combustion in a rocket elbow cookstove

The study began with a significant effort dedicated towards identifying and understanding the parameters that may significantly influence the $PM_{2.5}$ emissions from a rocket elbow cookstove. It was found that stick spacing and firepower all have an effect on $PM_{2.5}$ emissions. It was also found that the incorporation of a pot skirt has a significant effect on thermal efficiency but an insignificant effect on emissions.

The first variable studied was stick spacing. A consistent stick spacing of ½" was found to reduce emissions when compared to allowing the sticks to fall naturally together along the curved grate of the M5000. It was observed that in regions where sticks are touching or nearly touching, combustion may not occur. As pyrolysis gas is released from the fuel and enters regions of tight spacing, large fuel rich regions may be formed along the sides of the sticks and may contribute to particle nucleation and growth. Thus, if repeatable $PM_{2.5}$ emissions measurements are desired, consistent stick spacing should be maintained throughout all tests.

The next item that was studied was the addition of a pot skirt. The addition of a pot skirt to the M5000 led to an increase in thermal efficiency and slightly reduced, although not statistically significant, $PM_{2.5}$ emissions in terms of $PM_{2.5}$ per energy delivered. This suggests that a pot

skirt will be beneficial to general stove performance, but may not be critical to improving emissions performance.

The most significant discovery was the effect that firepower has on $PM_{2.5}$ emissions. It was found that varying the firepower causes significant variation in cold start WBT $PM_{2.5}$ emissions, with a nearly exponential relationship. This indicates that firepower, which is largely defined by the user's feed rate and fuel characteristics, should be a major variable of concern in the characterization of a stove's emissions. Consequently, a technique for correcting $PM_{2.5}$ emissions to some nominal firepower is proposed. Additionally, it was found that $PM_{2.5}$ emissions rates are significantly different within a WBT, with the start-up emissions generally contributing to a largely portion of the total emissions than the steady state phase emissions. This suggests that start-up procedures are extremely important to the characterization of cookstoves emissions, and that uniform start-up procedures should be defined for similar stoves.

11.2 Optimization of Methods for PM emissions reduction

The use of a forced draft system in a rocket elbow cookstove $PM_{2.5}$ emissions was explored. Two major approaches were tested. The first approach was exhaust gas recirculation, a novel technique for biomass cookstoves. A nozzle/flow rate optimization procedure was developed to enable rapid experimental progress. Three iterations of the optimization procedure with EGR resulted in a $PM_{2.5}$ emissions decrease of 44% from the M5000 baseline values.

Testing was completed to determine the isolated magnitudes of the driving mechanisms behind the observed 44% decrease in emissions. It was found that the isolated effects of elevated oxygen concentration in the flame above the fuel, increased residence time of particles in the flame, and enhanced mixing all contributed to a reduction in emissions. The effects of flame temperature reduction and dilution, and increased fuel consumption rate led to increases

in emissions, and the effect of carbon dioxide recirculation had no significant effect on emissions.

A comparison was then made between EGR and air injection. The same nozzle configuration that led to a 44% decrease in emissions with EGR was used. With this same configuration, air injection led to a 70% decrease in $PM_{2.5}$ emissions, indicating that air injection outperforms EGR for the case of the approximately 3kW wood burning rocket elbow cookstove.

Although, it was found that air injection will outperform EGR for this case, it may be hypothesized that EGR may outperform air injection for much larger stoves with higher flame temperatures. In the case of a larger stove with a hotter flame temperature, as seen with the Envirofit Institutional stove, the cooling effect of EGR may be used as a means to control the total draft through a stove, similar to the effect of a chimney. However, EGR will have the added benefit of simultaneously enhancing mixing and recirculating particles. Further testing of this hypothesis will complete the characterization of EGR as applied to biomass cookstoves.

Further iterations of the nozzle/flow rate optimization procedure using air injection were completed in an effort to understand and optimize key design parameters. Firstly, it was found that understanding the emissions as a function of the air injection flow rate is important. Although the emissions generally decrease as the flow rate increase, local peaks in emissions were observed at less than optimized flow rates. Also, the understanding the flow rate's upper limitations ensure that a product is designed that is practical and user-friendly.

It was found that injection location and injection angle are two very important parameters. Both of these factors are strong determinants of the optimized flow rates, upper limitations and the flow rates, and overall emissions performance. The highest performing injection locations were near at the top of the combustion chamber and at the bottom of the chimney. Both of these locations inject near the bottom of the flame, where it is strongest, but do not blow directly onto the fuel. The optimized flow rates for injection at the top of the combustion chamber were

higher than the optimized flow rates for injection at the bottom of the chimney. This is because quenching of the flame is more of a concern in the chimney, where the forced draft injection is more concentrated.

Nozzle diameters ranging from approximately 2 to 5 mm were tested for the top of the combustion chamber injection location using the side injection nozzles. It was found that diameters within this range did not significantly affect the optimized emission performance, but did have a slight effect on optimized flow rates, with the optimized flow rate tending to decrease as the diameter deceased. Additionally it was found that variation of the steady state phase air injection velocity from 5 to 20 meters/second with the various combinations of diameters and optimized flow rates had little effect on the emissions reduction.

Nozzle diameters from 1.5 to 3 mm were tested for the bottom of the chimney injection location. It was found that, when injecting forced draft into the chimney of the stove, the nozzle diameters is a strong determinant of the optimized emissions and flow rates. Larger diameters nozzles in this location tend to quench the flame, ultimately limiting the optimized flow rates and limiting the emissions reduction.

Ultimately, this analysis proved that significant $PM_{2.5}$ emissions reductions are possible through the use of air injection. The highest performing configuration, installed in the G3300, was a chimney ring nozzle that injected horizontally into the bottom of the chimney using 12 holes with 1.5 mm diameters. The optimized flow rates for this configuration were 20 to 40 SLPM for the start-up and steady state phases, respectively. The optimized $PM_{2.5}$ emissions were 61 (mg/MJ_d). This is an 84% decrease from the baseline G3300 $PM_{2.5}$ emissions, and a 94% decrease from traditional stove $PM_{2.5}$ emissions [4].

11.3 Design Recommendations

Out of all of the configurations tested, one in particular stood out not only for its high performance, but also for its practicality. This is the chimney ring nozzle with 12 holes with 1.5 mm diameters, angled horizontally and located at the bottom of the chimney of the G3300. This configuration resulted in an 84% reduction in emissions when using compressed air and a 78% reduction when using a Micronel 5V radial blower powered at 2 watts. When the Micronel radial blower was used, less the maximum flow rate achieved was approximately 12 SLPM. However, the optimized flow rates for this configuration were 20 to 40 SLPM for the startup and steady state phases. The 78% reduction realized at a flow rate of 12 SLPM indicates that the performance of this configuration is not highly sensitive to the use of less than optimized flow rates.

This configuration is considered to be the most practical out of the other high performing configurations because it does not intrude into the combustion chamber. This removes the potential for injected air to blow directly onto the fuel, which would result in poor emissions performance and difficulty in maintaining combustion. Additionally, this configuration resulted in a 37% decrease in time to boil from the baseline G3300, an attribute that may is particularly valuable to the end user.

A disadvantage with this configuration is the small hole diameter. The 1.5mm hole diameter can lead to difficulties in achieving the significant flow rates, issues with cooling of the cold side TEG, and difficulties in manufacturing. However some potential solutions do exist. The range of diameters tested was 1.5 mm to 3.0 mm, where 1.5 mm led to an optimized reduction of 84% and the 3.0 mm led to an optimized reduction of 72% but observed quenching of the flame. It may be speculated that increasing the diameter to approximately 2.0 or 2.5 mm will not significantly decrease the performance but may allow for additional cooling of TEG cold side heat sink. Additionally, 2.0 mm is the general limit in Envirofit's manufacturing processes where

holes can be punched rather than drilled. Thus, it will be valuable to test 1.5, 2.0 and 2.5 mm diameter nozzles in the final prototype.

11.4 Potential for Impact

The impressive emissions reduction achieved in the laboratory indicates that this technology has the potential for significant health and environmental benefits, similar to those achieved with well performing gasifiers [4]. Preliminary testing was completed to prove that the laboratory performance could translate well to field performance. This testing indicated that with proper fan selection and Thermoelectric generator (TEG) design, a large emissions reduction may also be achieved in the field.

Design for consumer acceptance and design for manufacturability were considered throughout the duration of this study. The final recommended configuration is user friendly, manufacturable on a large scale, and provides the added benefit of significant cooking time savings.

11.5 Future Work

11.5.1 Effect on particle size distribution and chemical composition

In this study, the various parameters were optimized for particulate mass emissions reductions. General correlations exist between atmospheric particulate mass concentrations and human health. Particulate mass is only part of the equation though, as size distribution and chemical composition are also significant determinants of health and climate effects. For example, ultrafine particles (less than 0.1 microns) do not contribute significantly to particulate mass, but they can penetrate deeper into human airways and be absorbed and transported more effectively into the blood stream. Additionally, the propensity of soot to act as cloud

condensation nuclei is strongly related to particle number density and surface chemical composition [3].

Currently, the community's quantitative understanding of the effect of particle size and chemical composition on health is not well defined, but is rapidly expanding. Future testing of the effect of air injection and EGR on particle size and chemical composition is highly recommended, especially before release of the any consumer product.

11.5.2 Commercialization

Included in the scope of this project is successful commercialization of the emissions reducing technology. In order to achieve this goal, the technology will be incorporated into an Envirofit product line. Several steps must be taken before the product is ready for sale. These include TEG design, electronics design, design for manufacturability, and field and durability testing. The first generation TEG and circuitry design is expected to be completed by April of 2015. The goal with design of the TEG and associated circuitry is to ensure that enough power is provided to the blower, to use any surplus power for cellphone and/or LED light charging via a 5 V USB port, and to store the remainder in a battery pack. Field and durability testing of the product is scheduled to begin in April of 2015 in Envirofit testing facilities in India. The stove will undergo 5,000 hours of burn time, during which temperature and power data will be logged. An early stage example prototype is pictured in Figure 42.

Figure 42. First Generation Air Stove Prototype

REFERENCES

[1] Kshirsagar, M., & Kalamkar, V. (2013). A comprehensive review on biomass cookstoves and a systematic approach for modern cookstove design. Renewable and Sustainable Energy Reviews, 30, 580-603.

[2] Household air pollution and health. (2014, March 1). Retrieved March 3, 2015, from http://www.who.int/mediacentre/factsheets/fs292/en/

[3] Wang, H. (2011). Formation of nascent soot and other condensed-phase materials in flames. Proceedings of the Combustion Institute, 33, 41-67.

[4] Stove Performance Inventory Report. (2012). Berkley Air Monitoring Group.

[5] Lightly, J., Veranth, J., & Sarofim, A. (2000). Combustion Aerosols: Factors Governing Their Size and Composition and Implications to Human Health. Journal of the Air & Waste Management Association, 50, 1565-1618.

[6] Influence of stove type and cooking pot temperature on particulate matter emissions from biomass cook stoves. (2012). Energy for Sustainable Development, 16, 448-455.The Water Boiling Test", Version 4.2.3

[7] The effect of oxygen and carbon dioxide concentration on soot formation in non-premixed flames. (2005). Fuel, 85, 615-624.

[8] Stanmore, B., Brilhac, J., & Gilot, P. (2001). The oxidation of soot: A review of experiments, mechanisms and models. Carbon, 39, 2247-2268.

[9] The Water Boiling Test Version 4.2.3. (2014). The Global Alliance for Clean Cookstoves.

[10] Guidelines for Data Acquisition and Data Quality in Evaluation in Environmental Chemistry. (1980). Analytical Chemistry, 52, 2242-2249.

[11] Devore, J. (2008). Probability and Statistics for Engineering and the Sciences (7th ed.). San Luis Obispo, CA: Thomson Brooks/Cole.

[12] Agenbroad, J., DeFoort, M., Kirkpatrick, A., & Kreutzer, C. (2011). A Simplified Model for Understanding Natural Convection Driven Biomass Cooking Stoves-Part 2: With Cook Piece Operation and the Dimensionless Form. Energy for Sustainable Development, 15, 169-175.

[13] Wijayanta, A., Alam, S., Nakaso, K., Fukai, J., & Shimizu, M. (2012). Optimized Combustion of Biomass Volatiles by Varying O2 and CO2 Levels: A Numerical Simulation Using a Highly Detailed Soot Formation Reaction Mechanism. Bioresource Technology, 110, 645-651.

[14] Miller-Lionberg, D. (2011). A Fine Resolution CFD Simulation Approach for Biomass Cook Stove Development. Fort Collins, CO.

[15] Williams, A., Jones, J., Ma, L., & Pourkashanian, M. (2011). Pollutants from the combustion of solid biomass fuels. Progress in Energy and Combustion Sciences, 38, 113-137.

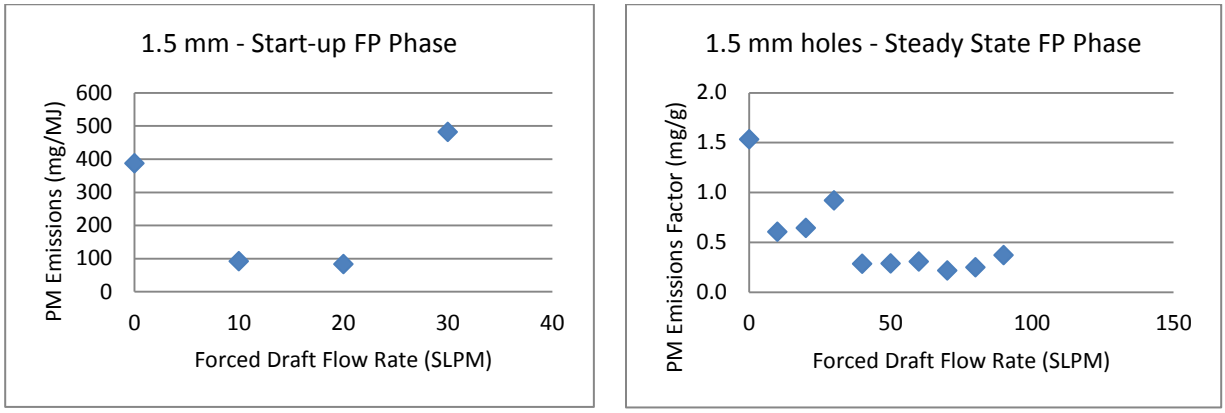

Figure 43. G3300 Side Injection Nozzles 1.5 mm Diameter Flow Rate Optimization

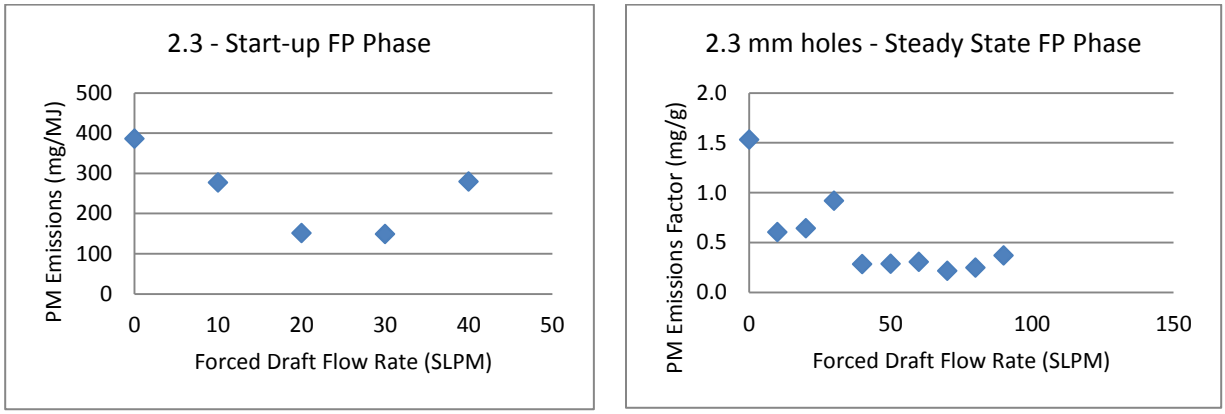

Figure 44. G3300 Side Injection Nozzles 2.3 mm Diameter Flow Rate Optimization

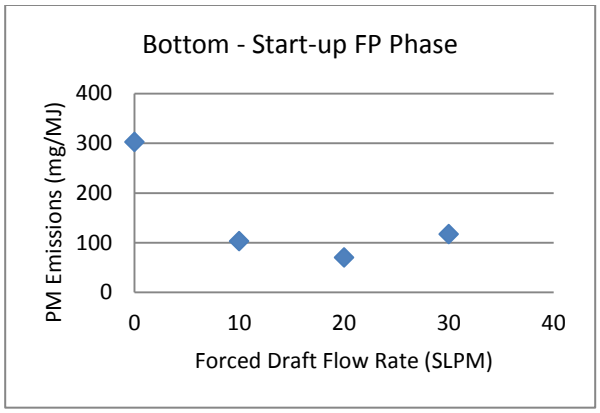

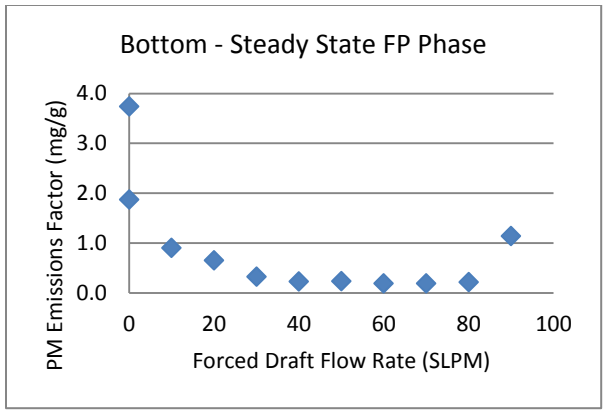

Figure 45. G3300 Chimney Ring at Bottom with 1.5 mm Diameter Flow Rate Optimization

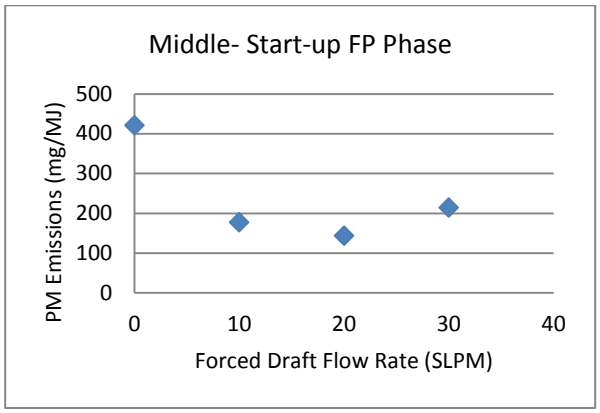

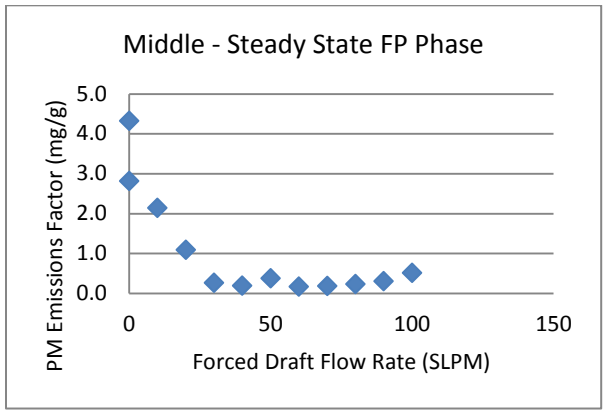

Figure 46. G3300 Chimney Ring at Middle with 1.5 mm Diameter Flow Rate Optimization

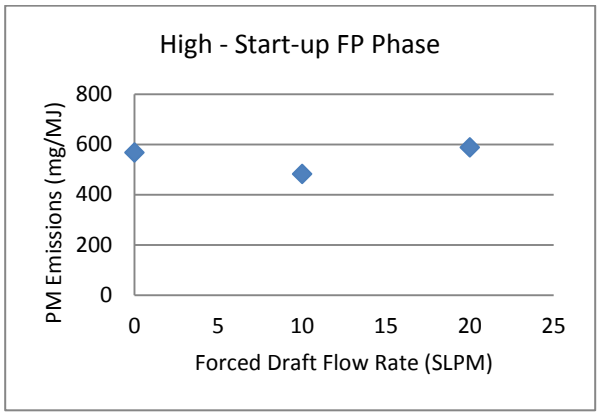

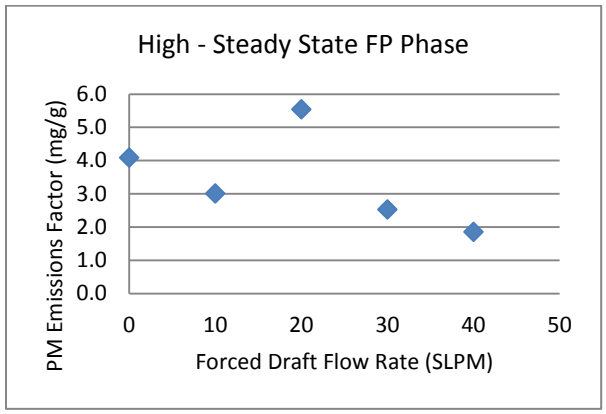

Figure 47. G3300 Chimney Ring at Top with 1.5 mm Diameter Flow Rate Optimization

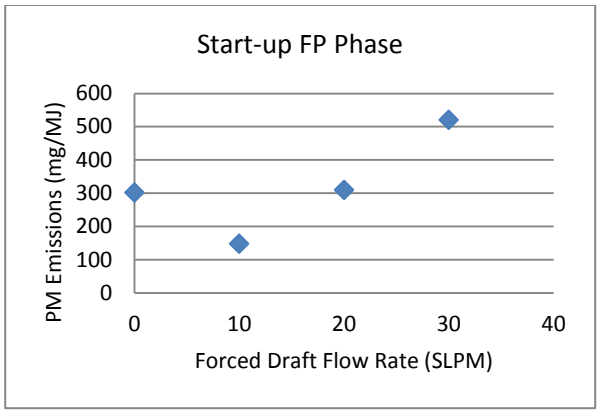

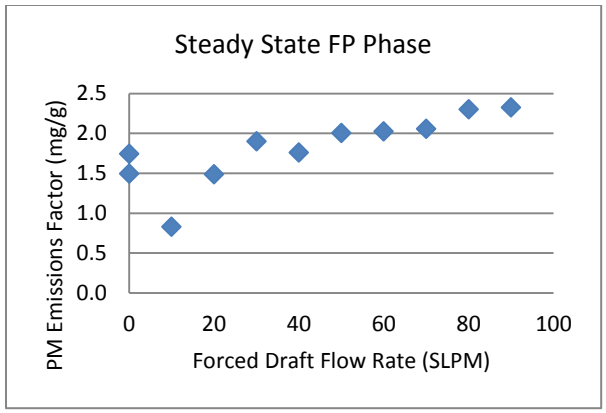

Figure 48. G3300 Chimney Ring at Bottom with 1.5 mm Diameter and 30^{O} Angle Flow Rate Optimization

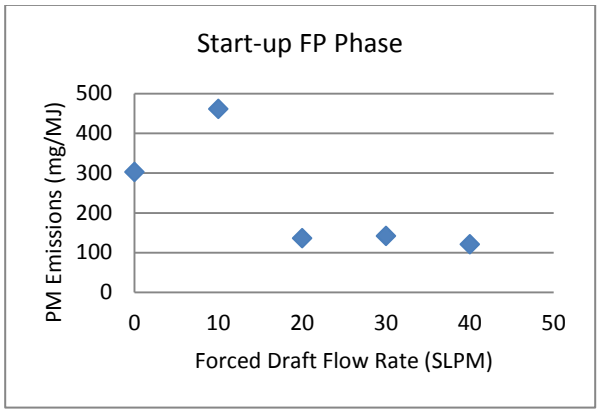

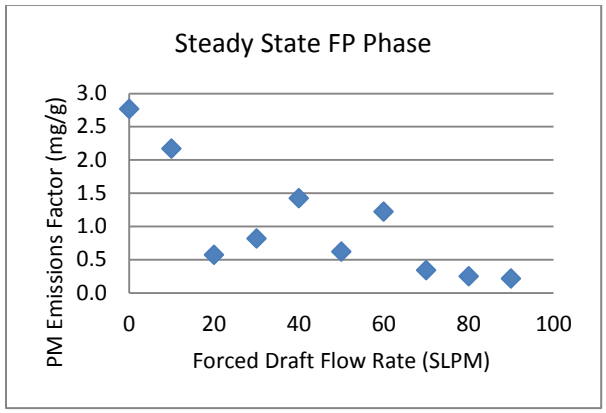

Figure 49. G3300 Chimney Ring at Bottom with 3.0 mm Diameter Flow Rate Optimization